

Recent updates on g-C₃N₄/ZnO-based binary and ternary heterojunction photocatalysts toward environmental remediation and energy conversion

Article history:

Received: 24-09-2023

Revised: 02-11-2023

Accepted: 15-12-2023

**Parul Rana^a, Sonu^b, Priya Dhull^c, Anita Sudhaik^d,
Akshay Chawla^e, Van-Huy Nguyen^f, Savaş Kaya^g,
Tansir Ahamad^h, Pardeep Singhⁱ,
Chaudhery Mustansar Hussain^j, Pankaj Raizada^k**

Highlights

- The properties of g-C₃N₄ and ZnO as photocatalytic materials were discussed.
- Several modification strategies were explored to improve photocatalytic performance.
- Synergistic effect among g-C₃N₄/ZnO boosted charge separation and light responsiveness.
- g-C₃N₄/ZnO-based nanocomposite exhibited reduced agglomeration and photocorrosion for longevity.
- Photocatalytic applications of g-C₃N₄/ZnO-based photocatalysts were explored.

ABSTRACT

Background: The utilization of photocatalytic materials has garnered significant consideration due to their distinctive properties and diverse applications in environmental remediation and energy conversion. In photocatalysis, several wide and narrow band gap photocatalysts have been discovered. Amongst several photocatalysts, g-C₃N₄ photocatalyst is becoming the interest of the research community due to its unique properties. But as a single photocatalyst, it is inherited with certain confines for instance higher photocarrier recombination rate, lower quantum yield, low specific surface area, etc. However, the heterojunction formation of g-C₃N₄ with other wide band gap photocatalysts (ZnO) has improved its photocatalytic properties by overcoming its limitations.

Methods: The synergistic interaction amid g-C₃N₄ and ZnO photocatalysts enhanced optoelectrical properties superior mechanical strength and improved photocatalytic activity. The nanocomposite exhibits excellent stability, high surface area, efficient separation, and migration of photocarriers, which are advantageous for applications in photocatalytic energy conversion and environmental remediation. The g-C₃N₄-ZnO nanocomposite represents a material comprising g-C₃N₄ and ZnO photocatalysts which exhibit a broad absorption range, efficient electron-hole separation, and strong redox potential. The combination of these two distinct materials imparts enhanced properties to the resulting nanocomposite, making it suitable for various applications. Henceforth, current review, we have discussed the photocatalytic properties of g-C₃N₄ and ZnO photocatalysts and modification strategies to improve their photocatalytic properties.

^a School of Advanced Chemical Sciences, Shoolini University, Solan, HP 173229, India.

^b School of Advanced Chemical Sciences, Shoolini University, Solan, HP 173229, India.

^c School of Advanced Chemical Sciences, Shoolini University, Solan, HP 173229, India.

^d School of Advanced Chemical Sciences, Shoolini University, Solan, HP 173229, India.

^e School of Advanced Chemical Sciences, Shoolini University, Solan, HP 173229, India.

^f Chettinad Hospital and Research Institute, Chettinad Academy of Research and Education (CARE), Kelambakkam, Kanchipuram District, 603103, Tamil Nadu, India.

^g Sivas Cumhuriyet University Health Services Vocational School Department of Pharmacy 58140 Sivas Turkey.

^h Department of Chemistry, College of Science, King Saud University, Saudi Arabia.

ⁱ School of Advanced Chemical Sciences, Shoolini University, Solan, HP 173229, India.
Corresponding Author:
Pardeepchem@gmail.com

^j Department of Chemistry and Environmental Science, New Jersey Institute of Technology, Newark, NJ 07102, USA.

^k School of Advanced Chemical Sciences, Shoolini University, Solan, HP 173229, India.
Corresponding Author:
Pankajchem1@gmail.com.

Significant Findings: This article offers an inclusive overview of the g-C₃N₄-ZnO-based nanocomposite, highlighting its photocatalytic properties and potential applications in several pollutant degradation and energy conversion including hydrogen production and CO₂ reduction

Keywords: Photocatalysis; g-C₃N₄; ZnO; Pollutant degradation; Hydrogen production; CO₂ reduction.

1. INTRODUCTION

Wastewater effluents from industrial pilot plants and country farmland are significant contributors to the pollution of natural water with poisonous organic chemical substances, such as organic colors and pesticides, contributing to the global crisis (Karri *et al.*, 2021; Pandey *et al.*, 2021). The escalating water pollution crisis threatens aquatic ecosystems and human health, while the unsustainable energy consumption crisis exacerbates environmental degradation and climate change. Humanity may face a shortage of potable water as a result of climate change and global warming, in addition to the impacts caused by human actions (Belhassan, 2021). Due to water shortages caused by climate change and bad water resource management, the adoption of water recycling and reuse has gained fast focus worldwide in recent years. Adsorption, membrane separation, and coagulation are just some of the methods used to clean water and get rid of organic pollutants, however, they only consolidate or transform the toxins into a solid form rather than getting rid of them (Shrestha *et al.*, 2021). Therefore, renewing the adsorbents and handling the secondary contaminants at an additional expense is necessary (Li *et al.*, 2019; Vinayagam *et al.*, 2022; Younas *et al.*, 2021). To get rid of persistent organic contaminants, particularly those with poor biodegradability, advanced oxidation processes (AOPs) have been suggested (Badmus *et al.*, 2018). In AOPs, the generation of [•]OH (hydroxyl radicals) and the regeneration of ions determine the pace of the degradation/oxidation process (Nidheesh *et al.*, 2022; Titchou *et al.*, 2021). Hydroxyl ([•]OH) radicals are powerful oxidants that can oxidize even the most resistant chemical substances. AOPs have many benefits, including (i) a high rate of decomposition, (ii) the conversion of organic compounds to environmentally friendly products, (iii) the ability to function in environments with low temperature and pressure as well as (iv) reduction of organic compounds' toxicity (Liu, L. *et al.*, 2021).

In recent years, the field of photocatalysis has gained significant attention due to its potential applications for environmental pollution and energy

sustainability (Chawla *et al.*, 2023). Photocatalysis is a process in which light energy is used to initiate chemical reactions by exciting the valence band (VB) electrons of a photocatalyst material to higher energy levels i.e. conduction band (Ameta *et al.*, 2018). Once the electrons are excited, they can participate in redox reactions, resulting in the photodegradation of pollutants or the production of clean energy sources. The efficiency and effectiveness of photocatalysis depend on several factors, including the band structure, charge carrier dynamics, and surface properties of the photocatalytic materials (Gupta, 2017). Photocatalytic materials, which can harness solar energy to drive chemical reactions, have emerged as promising candidates for various applications, including wastewater treatment, air purification, and solar fuel production (Bai *et al.*, 2019; Coronado *et al.*, 2013). Silver nanoparticles and gold nanoparticles are nanomaterials known for their exceptional photocatalytic properties to remove pollutants from wastewater (Kumar, 2021). When exposed to light, they can initiate photocatalytic degradation of various waste materials via surface plasmon resonance. These nanoparticles harness the energy from photons to generate reactive species, which efficiently break down the waste into harmless by-products, making them promising candidates for eco-friendly wastewater treatment and environmental remediation processes. Similarly, various natural green materials like chitosan, graphene, and cellulose-based derivatives are increasingly utilized in photocatalysis (Ambaye *et al.*, 2022; Chauhan *et al.*, 2023; Dutta *et al.*, 2019; Zheng *et al.*, 2022). These materials serve as excellent support matrices for photocatalysts, enhancing their stability and recyclability. They offer eco-friendly alternatives that can efficiently harness solar energy to drive chemical reactions for environmental remediation and energy production, promoting sustainability in photocatalytic applications. TiO₂ was first discovered in photocatalysts which has received the most research attention over the past several decades (Yan *et al.*, 2015). It has been widely used in the photodegradation of organic compounds under UV light sources because of its low fabrication cost and good chemical

stability (Pant *et al.*, 2019). For instance, Zhu and his co-workers synthesized In₂S₃ decorated with TiO₂ metastable phase of titania for the degradation of tetracycline (Zhu, C. *et al.*, 2022b). With a removal efficiency of 97.3%, the S-scheme In₂S₃/TiO₂ composite outperformed TiO₂ and In₂O₃ by 3.2 and 2.1 times, respectively. The S-scheme also preserves active sites for catalysis and delivers an internal electron channel at the interface. In another work to remove oxytetracycline hydrochloride photocatalytically, we design and build edge-rich bicrystalline 1T/2H-MoS₂ nanosheet co-catalyst modified V-doped hierarchical TiO₂ microspheres (Zhu, C. *et al.*, 2022a). An all-solid-state Z-scheme heterostructure is produced by the effective electron mediation provided by the metallic 1T phase of MoS₂. The V-TiO₂/1T/2H-MoS₂-5% heterojunction exhibits remarkable performance with a 92.4% photodegradation rate by concurrently boosting electron-hole separation, increasing reactive radical generation, expanding visible light absorption, and improving reactant adsorption capacity. According to Wang *et al.*, the wide band gap (3.2 eV) and poor quantum efficiency of TiO₂ severely limit its use in solar energy applications. Besides TiO₂, different kinds of photocatalytic materials have been discovered which have been categorized into narrow and wide band gap photocatalysts (Jiang *et al.*, 2018; Liu, J. *et al.*, 2021; Zhu, L. *et al.*, 2018). Among these materials, the combination of graphitic carbon nitride (g-C₃N₄) and zinc oxide (ZnO) has garnered considerable interest as a nanocomposite nanomaterial with enhanced photocatalytic performance and versatility (Lee *et al.*, 2022; Sayed *et al.*, 2022; Sun *et al.*, 2022).

g-C₃N₄ (metal-free photocatalyst) is one of the most potentially visible-light-responsive materials that have a cheap cost, environmental tolerance, good stability, and simple production (Abu-Sari *et al.*, 2023; Rajeshwari *et al.*, 2022). Furthermore, it is an excellent substance for photocatalytic activity due to its mix of artificial and organic features. It contains carbon and nitrogen atoms arranged in a two-dimensional layered structure, resembling graphene (Wang *et al.*, 2020). The electronic band structure of g-C₃N₄ allows it to absorb visible light, enabling efficient utilization of solar energy. The small band gap (2.7 eV) of g-C₃N₄ allows it to make better use of solar energy (Dutta *et al.*, 2023; Hayat *et al.*, 2022). A polymeric carbon nitride material has appeared as a popular choice for photocatalytic applications due to its unique electronic structure

and chemical stability (Kumar *et al.*, 2023; Wei *et al.*, 2022). For example, Le *et al.* successfully synthesized the S scheme V₂O₅/g-C₃N₄ for eliminating harmful antibiotic residues with an efficiency of 91.3% (Le *et al.*, 2022). An internal electron channel is provided at the interface by the V₂O₅/g-C₃N₄ S-scheme structure, which also keeps the active sites with high photodegradation potentials. Our research provides strong V₂O₅/g-C₃N₄ S-scheme nanocomposite for environmentally friendly water filtration. Additionally, high chemical and thermal stability make g-C₃N₄ suitable for various reaction conditions. On the other hand, ZnO, a wide-band-gap semiconductor, has long been recognized as a photocatalyst with excellent properties. ZnO is an n-type silicon oxide like TiO₂, but it has received less attention in the past. Since, ZnO shares the same energy gap energy as TiO₂ but, displays greater absorption efficacy across a significant portion of the solar spectrum, it has been suggested as a replacement photocatalyst for TiO₂. ZnO possesses a direct band gap energy that allows the absorption of ultraviolet (UV) light, making it highly effective in harnessing solar radiation (Bulcha *et al.*, 2021). Owing to the aforementioned unique and advantageous properties, both g-C₃N₄ and ZnO photocatalysts have been considered efficient materials for environmental remediation, but as a single photocatalyst, they exhibit several limitations that affect their photocatalytic performance. However, the photoefficiency of g-C₃N₄ and ZnO photocatalysts in photocatalysis is constrained by several issues. For instance, g-C₃N₄ has restricted photocatalytic activity, narrow light absorption range, charge carriers fast recombination, poor stability, and lower specific surface area (Pattanayak *et al.*, 2023), etc. Similarly, ZnO as a wide band gap photocatalyst also has certain constraints such as charge carriers recombination rate, limited selectivity, restricted light absorption range (absorption of UV spectrum), photocorrosion and material degradation, etc. which have limited its photoactivity (Ahmad *et al.*, 2022). In visible light, both materials could only show a small amount of photocatalytic activity. Long-term efficiency may also be impacted by their photocorrosion and stability in challenging environments. Moreover, these photocatalysts' total catalytic effectiveness may be hampered by the recombination of photo-generated electron-hole pairs, therefore it is imperative to discover practical ways to alleviate these constraints.

Therefore, the integration of $g\text{-C}_3\text{N}_4$ and ZnO represents a remarkable combination of semiconductors with distinct advantages. By combining $g\text{-C}_3\text{N}_4$ and ZnO, a nanocomposite nanomaterial is formed, harnessing the individual strengths of each component (Ma *et al.*, 2019). Various synthesis methods, such as solvothermal methods, hydrothermal synthesis, and co-precipitation techniques, have been employed to fabricate $g\text{-C}_3\text{N}_4/\text{ZnO}$ -based nanocomposite with controlled morphology, composition, and surface properties (Kumaresan *et al.*, 2020; Liu *et al.*, 2019; Luu Thi *et al.*, 2021; Yu, T. *et al.*, 2022). The combined effects between $g\text{-C}_3\text{N}_4$ and ZnO lead to enhanced photocatalytic performance, extended light absorption range, improved charge separation, and increased surface area for active sites, making it a promising candidate for environmental and energy applications. The unique band structures of $g\text{-C}_3\text{N}_4$ and ZnO allow the absorption of both visible and UV light, enabling efficient exploitation of solar energy across a broad spectrum (Jung *et al.*, 2019). This broad light absorption range is crucial for practical applications, as it maximizes the utilization of sunlight, which is the most abundant and sustainable energy source available. Moreover, the favorable band positioning between $g\text{-C}_3\text{N}_4$ and ZnO promotes efficient charge separation, reducing the chance of recombination between photogenerated electron-hole pairs. This charge separation efficiency significantly enhances the photocatalytic activity and contributes to improved reaction rates (Liu, B. *et al.*, 2021; Sayed *et al.*, 2022). Additionally, the large surface area of the nanocomposite nanomaterial provides abundant active sites for organic/inorganic pollutant adsorption, increasing the opportunities for catalytic reactions. The versatile nature of $g\text{-C}_3\text{N}_4/\text{ZnO}$ nanocomposite extends their applicability to various environmental and energy-related domains (Huang *et al.*, 2021; Liu, B. *et al.*, 2021; Sayed *et al.*, 2022).

Here, in this article, we provide a high-level introduction to $g\text{-C}_3\text{N}_4$ -based ZnO photocatalyst so that readers can grasp the fundamentals of microstructural matching between $g\text{-C}_3\text{N}_4$ and ZnO for photocatalytic activity. In this context, $g\text{-C}_3\text{N}_4$ and ZnO-based photocatalytic materials have been discovered with their potential applications for pollutant degradation and energy conversion (Alharthi *et al.*, 2020; Liu, J. *et al.*, 2020). By harnessing solar energy, these materials can effectively degrade organic pollutants and convert harmful compounds

into harmless substances (Sun *et al.*, 2022; Zhang, S. *et al.*, 2019). The unique properties of $g\text{-C}_3\text{N}_4/\text{ZnO}$ nanocomposite make them highly effective in various energy conversion processes, including water splitting, hydrogen production, and carbon dioxide reduction (Ge *et al.*, 2023; Liu, B. *et al.*, 2021; Sayed *et al.*, 2022). The synthesis and engineering of $g\text{-C}_3\text{N}_4/\text{ZnO}$ -based nanocomposites offer a wealth of opportunities to tailor their properties for specific applications (Liu *et al.*, 2018). These approaches allow for the optimization of material characteristics, such as band gap engineering, surface area, and charge carrier dynamics, to achieve superior photocatalytic performance. Moreover, the incorporation of dopants and co-catalysts further enhances the activity and selectivity of $g\text{-C}_3\text{N}_4/\text{ZnO}$ nanocomposite, providing additional avenues for material design (Qamar *et al.*, 2022; Sun *et al.*, 2019). In conclusion, $g\text{-C}_3\text{N}_4/\text{ZnO}$ nanocomposite holds immense promise for environmental and energy applications. Their unique properties, synergistic effects, and versatile fabrication methods make them ideal candidates for addressing the challenges of environmental remediation

2. $g\text{-C}_3\text{N}_4$ (g-CN) PHOTOCATALYST

Ground-breaking research by Wang and co-workers on visible-light photo-catalytic water splitting over graphitic carbon nitride (g-CN) in 2009, g-CN has received a great deal of interest. It is generally agreed that, among the numerous carbon nitrides, g-CN is the highest balanced allotrope when exposed to room temperature and humidity (Sudhaik *et al.*, 2023). Fig. 1 demonstrates its suggested structure of tri-s-triazine two-dimensional frameworks linked by tertiary amines, g-CN is both chemically (at room temperature) and thermally (up to 600°C in the atmosphere) stable (Wang *et al.*, 2012). A polymeric metal-free photocatalyst, g-CN is being investigated for its potential use in the breakdown of organic contaminants in water. With its excellent chemical and thermal stability, sensitivity to visible light, and adequate band gap (2.7 eV), g-CN is a cost-effective photocatalyst that has been extensively employed for carbon dioxide (CO_2) reduction, hydrogen (H_2) evolution, organic synthesis, and organic pollutant elimination. This makes g-CN the undisputed leader in photocatalysis very instantly. There are several remarkable qualities of g-CN, including non-toxicity, stability, cheap cost, an acceptable energy gap, and visible-light absorption

(Malik *et al.*, 2021). Nonetheless, pure g-CN still has several flaws like low quantum yield, charge recombination, poor conductivity, etc., hence it is sometimes altered (Sharma *et al.*, 2022). Melamine or dicyandiamide thermal polycondensation/polymerization is a straightforward production process that yields g-CN. The process of thermal polymerization of urea may also be used to fabricate g-CN. Thermal polycondensation of melamine or dicyandiamide releases several harmful gases that might damage the environment, yet the process is straightforward (Barrio *et al.*, 2020). Unfortunately, the yield from urea thermal polymerization is low, and both the calcination environment and the temperature are strict. The use of g-CN as a photocatalyst for the degradation of MO and rhodamine

B (RhB) has been the subject of many published works (Fan *et al.*, 2022; Liu, N. *et al.*, 2020; Yu, B. *et al.*, 2022). For photodegradation, the holes and electrons are responsible, which breaking down dyes despite their high recycling efficiency and long-term stability. Bare g-CN has poor photocatalytic degradation capability because photogenerated e⁻-h⁺ charge carriers recombine at a high rate. To boost its photocatalytic capabilities, g-CN has been tested with a wide variety of additives in the past. They include Bi₂MoO₆, Ag₃PO₄, BiOBr, Bi₂Sn₂O₇, BiVO₄, BiOCl, and ZnO among others (Zhang *et al.*, 2018). The photocatalytic efficacy of g-CN has been enhanced in a variety of ways, including doping, crystal phase and facet management, and heterojunctions.

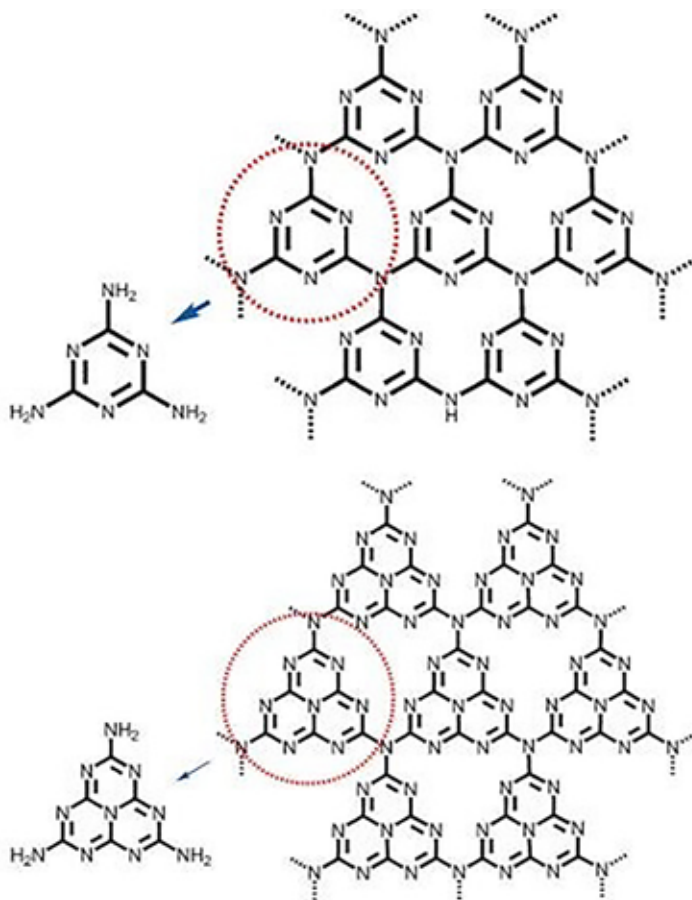


Figure 1. Structure of g-CN s-triazine (upper) and tri-s-triazine (down).

Adapted with permission from Elsevier (License No. 5583571189510) (Wang *et al.*, 2012).

2.1. Doping

Photocatalytic capabilities for dye removal have been boosted by doping g-CN with various

elements (Fronczak, 2020). Boron-doped mesoporous carbon nitride has been used, for instance, to detoxify malachite green. Doping with 1% boron was the most effective. At room temperature,

response surface methods projected that 18 mg of this sorbent would be able to remove 20 mg/L. Here, boron doping altered the electrical arrangement of g-CN, leading to an extreme density of surface charge. The strong acid-base contact between boron and g-CN presents a promising potential for basic dyes due to boron's Lewis acidic nature (Azimi *et al.*, 2019). To break down various dyes, boron has been doped with g-CN using a variety of techniques, including thermal and solvothermal ones (Sivaprakash *et al.*, 2021). Carbon doping, like boron doping, increases interaction and electrostatic attraction and leads to better degradation and adsorption of colors in wastewater. The maximum absorption of 57.87 mg/g within 300 min was reported by Ren *et al.* (Ren *et al.*, 2018). They utilized a C-doped g-CN photocatalyst for MB degradation. The reported C-doped g-CN composite revealed much higher photocatalytic efficacy than any other g-CN photocatalyst investigated to date, as shown in Fig. 2a. After that Phosphorus-doped g-CN has recently deteriorated MB. At pH 8, 60 min at 18 °C,

with an initial concentration of MB 0.07 resulted in a maximum adsorption efficiency of 100 mg/g (Chegeni *et al.*, 2020). The observed dye adsorption efficiency was much greater than that of carbon- and boron-doped g-CN. Oxygen doping in the g-CN lattice, for instance, may change the electron and energy band structure, therefore it can be used to improve g-CN efficiency. By doing so, we may expand the surface area, enhance the responsiveness to visible light, and better segregate photogenerated charge carriers. Doped g-CN was generated by Yang and Bian using a nitric acid ultrasonication technique, and it was able to degrade Rhodamine B by up to 93.88% after 2 hours and 100% after 3 h. in the occurrence of UV-light as shown in Fig. 2(b-d) (Yang *et al.*, 2021). Singlet oxygen, an additional effective portion in the redox process necessary for the breakdown of dye, was shown to be responsible for the improved photocatalytic efficacy. g-CN doped with non-metals such as sulfur and phosphorous has formed heterojunctions, improving the material's photodegradation properties.

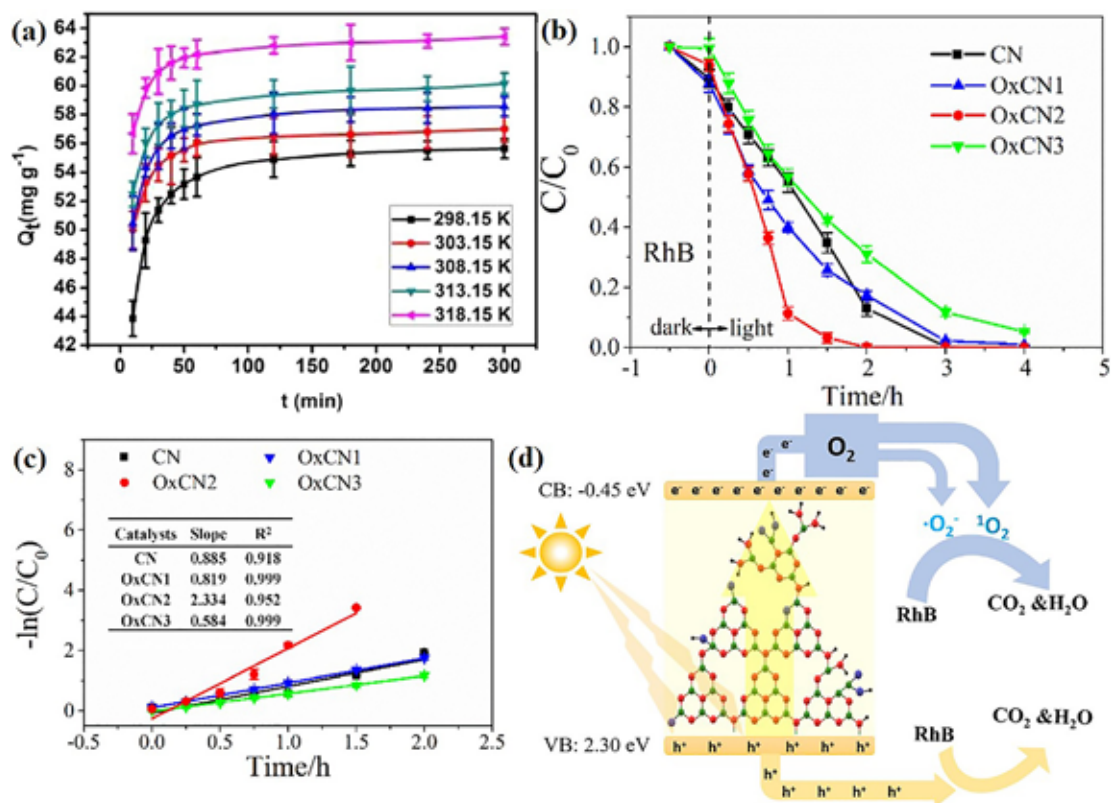


Figure 2. (a) At various temp. MB adsorption efficiency of doped g-C₃N₄. Adapted with permission from Elsevier (License No. 5585761278797) (Ren *et al.*, 2018), (b) Photodegradation efficiency of RhB dye, (c) pseudo 1st order kinetics fitting, and (d) Schematic illustration of photodegradation mechanism. Adapted with permission from Elsevier (License No. 5585770072959) (Yang *et al.*, 2021).

2.2. Structure facet and phase control

Structure facets and phases may be manipulated to modify the band gap and improve the photocatalytic characteristics of the material, which can be used alone or in conjunction with composite creation. Folded nonporous g-CN with improved energy band, crystal structure, and microstructure have been synthesized from urea using the calcination process modification to degrade MB as demonstrated in Fig. 3a (Li *et al.*, 2017). Decreased thickness, high porosity, and increased specific surface area (SSA) (197 m²/g) were the outcomes of using g-CN in this way. At temperatures between 450 °C and 500 °C, these characteristics were observed to improve. When heated to a further 550 °C, the pore structure vanished, and the material thinned out. This developed catalyst demonstrated a photocatalytic degradation rate for MB that was 9.9 times greater than bulk g-CN, with an efficiency of MB degradation reaching 98.5% after just 3 h (Fig. 3b). Folded g-CN had better performance, but it took too long to decompose

the dye to be practical. The thermal polymerization process reaction of melamine crystals created from a re-crystalline method obtained from transition metal ions led to the production of g-CN nanotubes, which enhanced the poor charge efficiency of g-CN. The produced crystals had a regular size of 20 nm on average, with facet (002) development being limited and other promising facets corresponding to (011), (210), and others showing promise (311). For improved photocatalytic activity, the crystal structure of g-CN was modified by the assignment of a tubular structure to it by changing metal ions. The axial direction of electron transmission is enhanced by a tubular shape (Jiang *et al.*, 2019). Ag inclusion with g-CN via 8 h. of calcination has a similar effect on crystallinity. An impressive MO degradation efficiency of 98% in 2 h was observed with the resultant Ag/CN-8 as demonstrated in Fig. 3(c-d) (Liu, R. *et al.*, 2020). The dispersibility of silver, SSA, and recombination rate of photoexcited e⁻-h⁺ were all improved by the calcination process, which also increased the visible light responsiveness.

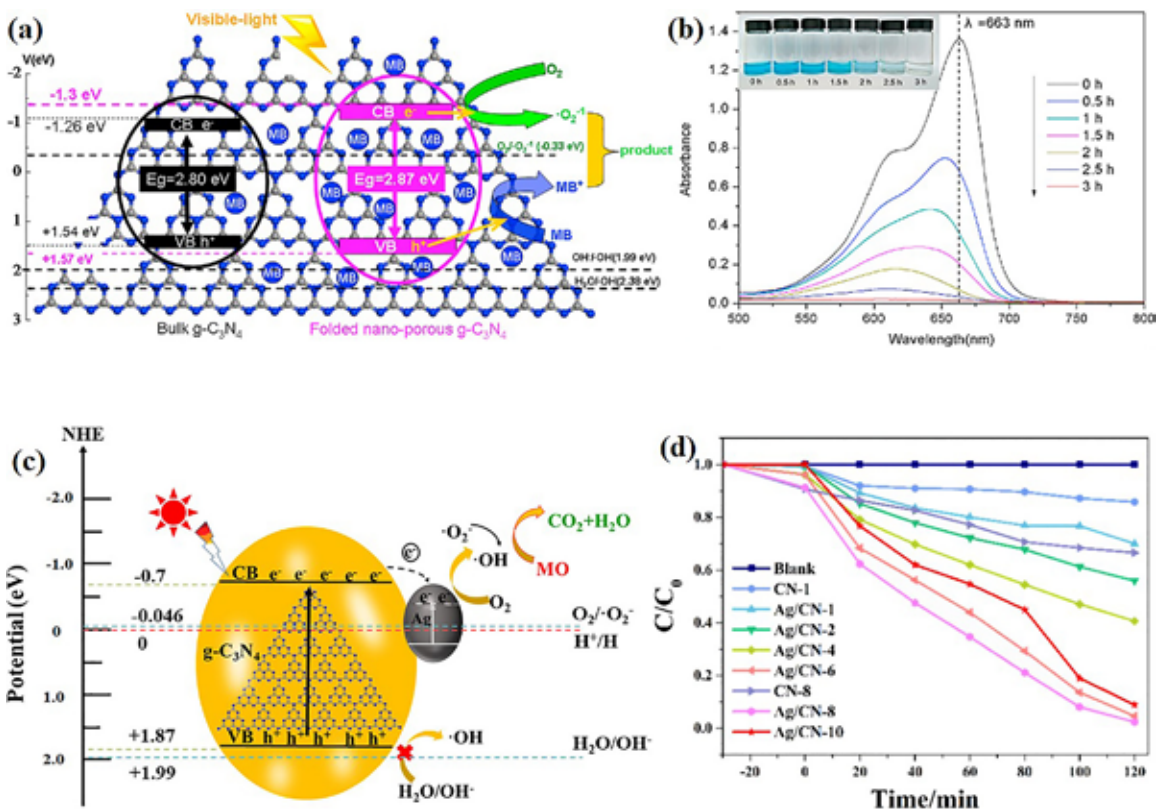


Figure 3. (a) Schematic representation of photodegradation of MB dye, (b) At various time intervals UV-visible spectra of MB dye degradation, Adapted with permission from Elsevier (License No. 5583631341989) (Li *et al.*, 2017), (c) Schematic illustration of photodegradation of 4-NP, (d) photodegradation 4-NP dye under visible light within 120 min, Open access (Liu, R. *et al.*, 2020).

2.3. Heterojunction

To boost the photodegradation efficiency of g-CN, researchers are working on heterojunction systems in which the oxidation and reduction capacities are enhanced by increasing the negative charge carrier binding energy of one component and increasing the positive charge carrier binding energy (VB) of another. Improved photocatalysis is achieved by using heterojunctions with components that have superior adsorption properties (He *et al.*, 2018; Xu *et al.*, 2019). To this end, it is crucial to develop and produce heterojunction-based photocatalysts with enhanced adsorption and degrading capabilities. $\text{La}_2\text{Ti}_2\text{O}_7$ was engaged to improve the heterojunction characteristics for better photocatalytic efficacy (Wang, F. *et al.*, 2017). $\text{La}_2\text{Ti}_2\text{O}_7$ have E_{CB} and E_{VB} around 0.39 eV and 3.33 eV band edges respectively are in good resonance with those of g-CN, facilitating the transfer of electrons from g-CN to $\text{La}_2\text{Ti}_2\text{O}_7$ as shown in Fig. 4a. As a consequence, these highly reducible electrons are used to generate a greater variety of active species. An effective composite photocatalyst for MB was created using g-CN and $\text{La}_2\text{Ti}_2\text{O}_7$. Hydrothermal synthesis of $\text{La}_2\text{Ti}_2\text{O}_7$ nanosheets and muffle furnace pyrolysis of melamine were employed to produce g-CN particles. Using a wet-impregnation technique, researchers designed a composite of g-CN powders and $\text{La}_2\text{Ti}_2\text{O}_7$ nanosheets with improved photocatalytic activity (90% MB was degraded in 2 h) as demonstrated in Fig. 4b. Yet, although the effectiveness was high, the time spent on it was excessive. Radical and hole-trapping studies were performed to study the function of active species (O_2^- , $\cdot\text{OH}$, h^+). Using the radical-quenching agent's isopropanol (IPA), $\text{Na}_2\text{C}_2\text{O}_4$, and benzoquinone (BQ), the researcher demonstrated that O_2^- and h^+ play an active part in the photocatalytic process. While TiO_2 is already a remarkable photocatalyst on its own, combining it with g-CN would likely boost its effectiveness even more, making it an ideal material for the photocatalytic destruction of organic contaminants. Fabrication of TiO_2 using MOF MIL-125 and preparation of g-CN through melamine were accomplished by Jia *et al.* Using the calcination technique, they created a Z-scheme g-CN/ TiO_2 nanocomposite (Jia *et al.*, 2020). Photodegradation of MB by g-CN/ TiO_2 nanocomposite was shown to be more effective than using either TiO_2 or g-CN. After testing various concentrations of g-CN, we found that 8wt% produced the

highest efficiency (97.7%) in less than 150 min as shown in Fig. (4c-d). As compared to g-CN, photocatalytic efficiency was enhanced, but it was still subpar. Subsequently, to effectively decompose RhB, MB, and BPA through photocatalysis when exposed to visible light, Sun and co-workers fabricated a new g-CN/ Bi_4O_7 Z-scheme heterojunction (Sun *et al.*, 2017). These g-CN powders originated from a muffle furnace thermal polycondensation of melamine. The hydrothermal approach was used to create Bi_4O_7 , and the calcination process was used to generate a composite with an increasing amount of g-CN. When g-CN was increased by another 10–30%, the photocatalytic performance improved, but the activity towards the destruction of dyes was observed to decrease at this point as demonstrated in Fig. 4g. Band gap narrowing in Bi_4O_7 and g-CN is responsible for the enhanced activity. By the interfacial heterostructure, electrons from Bi_4O_7 VB are transferred to CB, where they are excited, and then on to the VB holes in g-CN as demonstrated in Fig. 4h. Consequently, due to CB potential of g-CN (−0.95 eV) is more negative than that of O_2/O_2^- (−0.33 eV), dissolved molecular oxygen reacts with CB of g-CN electrons to create O_2^- . Nevertheless, the VB potential of Bi_4O_7 (+2.52 eV) is more than $\cdot\text{OH}/\text{OH}$ (+1.99 eV), and holes in VB of Bi_4O_7 oxidize OH to $\cdot\text{OH}$. The close relationship between g-CN and Bi_4O_7 was uncovered utilizing XRD, TEM, and SEM. Almost 90% dye degradation within 90 min by Bi_4O_7 /g-CN which is a long time and should be shortened. Table 1 shows the results of new research into the use of g-CN in combination with metal oxides and metal-organic frameworks for the effective degradation of pigments in water.

Due to their distinct electronic structures and malleable structural geometries metal oxides have recently emerged as a favorable material with significant potential as a photocatalyst. These characteristics allow them to function as semiconductors, metals, and insulators, respectively (Nemiwal *et al.*, 2021). Due to their cheap manufacturing cost, chemical stability, and ecologically benign, ZnO is the most researched compound among semiconductors for its use in dye-sensitized solar cells, photo-electrocatalysis of water, and environmental remediation. Yet their high band gap and poor quantum efficiency limit their use. Composite creation, dye sensitization, doping, metal/non-metal deposition, and surface modification are just some of the alterations that have been made to enhance photoactivity in the visible spectrum.

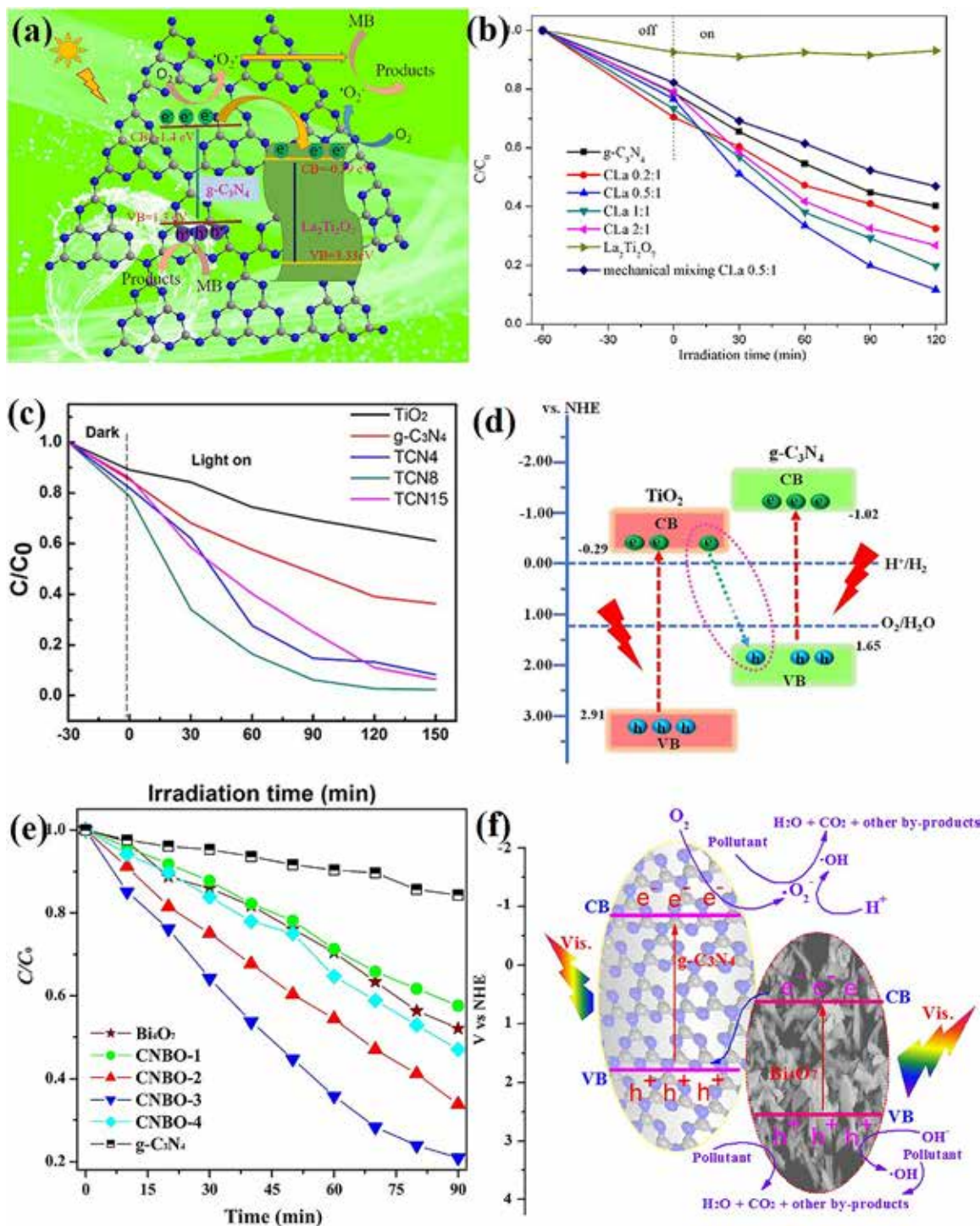


Figure 4. (a) Photodegradation efficacy of MB dye by fabricated nanoparticles, (b) Schematic diagram of photodegradation MB dye through heterojunction, Adapted with permission from Elsevier (License No. 5583640419845) (Wang, F. *et al.*, 2017), (c) Photodegradation efficacy of MB dye using fabricated nanoparticles, (d) Schematic illustration of photodegradation MB dye through heterojunction, Adapted with permission from Springer (License No. 501828549) (Jia *et al.*, 2020), (e) Photodegradation efficacy of MB dye by fabricated nanoparticles, and (f) Schematic illustration of photodegradation MB dye through heterojunction, Adapted with permission from Elsevier (License No. 5583641221023) (Sun *et al.*, 2017).

S. No.	Photocatalyst	Duration (min)	Pollutant	Degradation efficacy (%)	Reference
1	Ag ₃ PO ₄ /g-CN	20	RhB	99.98	(Deonikar <i>et al.</i> , 2019)
2	WO ₃ @ g-CN	90	RhB	99.5	(Borthakur <i>et al.</i> , 2020)
3	g-CN/H-ZSM-5	120	MB	92.7	(Barman <i>et al.</i> , 2020)
4	ZnO-Modified g-CN	80	MB	97	(Paul <i>et al.</i> , 2020)
5	g-CN/Bi ₄ O ₇	90	MB	90	(Sun <i>et al.</i> , 2017)
6	g-CN/Ag ₃ VO ₄ /β-AgVO ₃ /Ag	30	MB	95.5	(Joseph <i>et al.</i> , 2019)
7	g-CN/Co-MOF	80	CV	95	(Devarayapalli <i>et al.</i> , 2020)
8	LaFeO ₃ /g-CN	60	BB	100	(Wu <i>et al.</i> , 2018)
9	BiOCCOOH/ g-CN	120	Amido black 10B	89.16	(Cui <i>et al.</i> , 2019)
10	CeO ₂ /CNS	150	MB	91.4	(Jourshabani <i>et al.</i> , 2017)
11.	CdS/CQDs/g-CN	20	RhB	100	(Feng <i>et al.</i> , 2020)
12	MoS ₂ QDs/ g-CN	40	MO	96.3	(Shi <i>et al.</i> , 2018)
13	BiOI@UIO-66(NH ₂) @g-CN	80	RhB	95	(Liang <i>et al.</i> , 2018)

Table 1. Dye deterioration using a novel heterojunction of g-CN-based photocatalysts has recently found extensive application.

3. ZnO PHOTOCATALYST

Zinc oxide, or ZnO, is a very rare inorganic substance found in nature as the mineral zincite. It crystallizes into three different shapes: hexagonal wurtzite, cubic zinc blende, and cubic rock salt. ZnO often takes the wurtzite form, while rock salt and zinc blende are also infrequently seen (Batra *et al.*, 2022; Morkoç *et al.*, 2008). These latter structures are very metastable and hard to come by since they need high pressure and regulated development on cubic substrates. At room temperature and pressure, the hexagonal wurtzite phase is the most stable of all phases thermodynamically (Pathania *et al.*, 2021). Due to its improved tendency to crystallize in wurtzite form, ZnO has had the best photocatalytic efficiency focused on photocatalytic characteristics. ZnO crystalline formations are shown in Fig. 5 as a ball-and-stick model, with yellow spheres standing in for Zn atoms and blue

spheres for O atoms (Özgür *et al.*, 2013). Because of its potential to affect their behavior, nanomaterials' crystalline structure is an important characteristic. The band structure and optical transparency of ZnO, two crucial physicochemical features, are dictated by the atomic or molecular arrangement in a crystalline solid (Tudose *et al.*, 2019).

In hexagonal wurtzite structure lattice parameters, *a* and *c* are 0.3296 and 0.52065 nm respectively (Baruah *et al.*, 2009). Hexagonal sub lattice patterns are often used to illustrate the layered structure of the wurtzite ZnO, which consists of Zn²⁺ and O²⁻ ions alternatingly stacked along the *c*-axis. On the tetrahedral faces of each sub lattice, four Zn²⁺ ions are interspersed by four O²⁻ ions, and vice versa (George *et al.*, 2010). During the fabrication of ZnO nanostructures, ZnO has spontaneous polarization due to the generation of polar symmetry along the hexagonal axis, which originates from the tetrahedral coordination (Hughes *et al.*, 2004). As ZnO

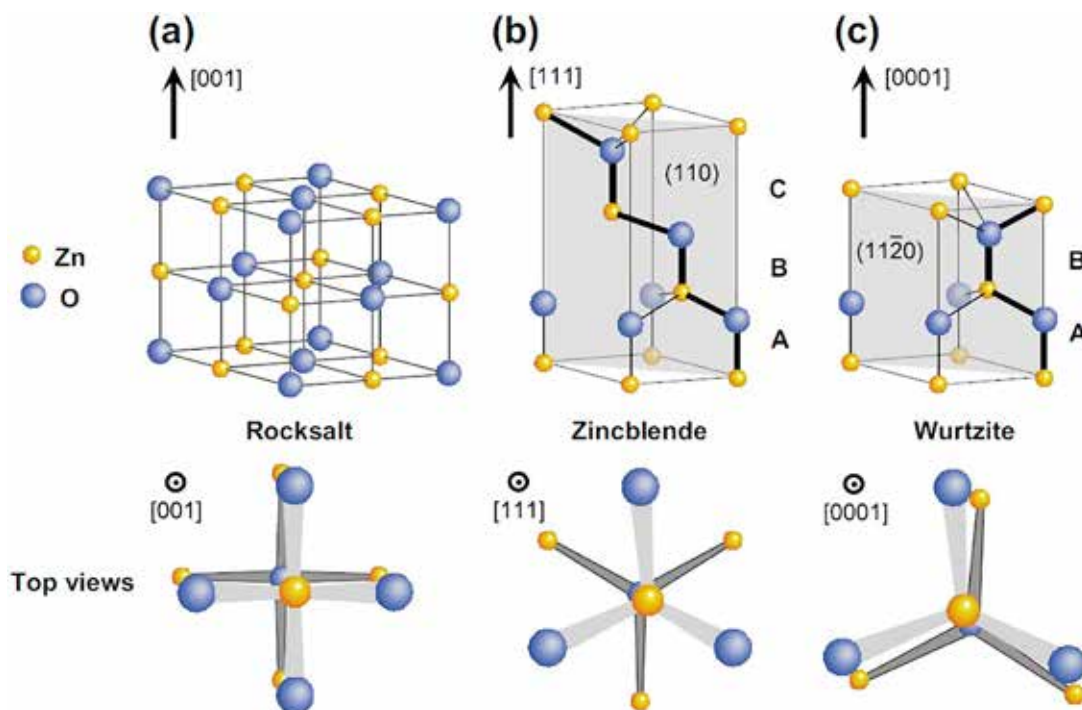


Figure 5. Zinc oxide crystals in stick-and-ball representation: (a) cubic rock salt (B1), (b) cubic zincblende (B3), and (c) hexagonal wurtzite (B4) Adapted with permission from Elsevier (License No. 5585770959074) (Özgür *et al.*, 2013).

lacks an inversion core of space groups, its non-centro-symmetric structure makes it piezoelectric and pyro-electric (Moore *et al.*, 2006). Both the Zn-(0001) and O-(0001) surfaces are typical polar surfaces in ZnO, but the (2 1 0 0 0) and (0 1 1 0 0) faces are non-polar surfaces with many O and Zn atoms and a minimal energy level (Sheikh *et al.*, 2020). Researchers have shown that studying the polarity of ZnO nanoparticles may help increase their efficacy as photocatalysts in the removal of contaminants from water under light. This may be achieved by adjusting the polarity of the photocatalyst and regulating the pace at which ZnO nanoparticles aggregate. ZnO nanoparticles can be categorized as either 0D, 1D, 2D, and 3D as demonstrated in Fig. 6a (Leonardi, 2017). Many synthesis approaches and synthesis kinetics affect ZnO nanostructure development. 0D ZnO arrays may have the form of quantum dots or hollow nanospheres, whereas 1D arrays can have the shape of nanofibers, nanorods, nanoneedles, nanotubes, nanobelts, and nanowires (Ahmad *et al.*, 2020; Cha *et al.*, 2018; Choi *et al.*, 2018; Imran *et al.*, 2017; Kennedy *et al.*, 2018; Kumar *et al.*, 2020; Thakur *et al.*, 2020). Nanosheets, nanoflakes, and disk-shaped formations are common examples of 2D nano architectures (Kanaparthi *et al.*, 2020;

Khera *et al.*, 2019; Manjula *et al.*, 2020; Wang, J. *et al.*, 2016). 3D arrays of ZnO nanostructures may take many forms, including flowers, urchins, and tetrapod's (Borbón *et al.*, 2019; Mishra *et al.*, 2018; Qu *et al.*, 2020; Wang, Y. *et al.*, 2016). Several ZnO morphologies in a range of diameters are shown in Fig. 6(b-j). ZnO physical, optical, electrical, and mechanical characteristics are strongly impacted by these morphologies, making them applicable to a wide range of sectors. As a result, effective photocatalytic performances need ZnO nanostructure designs for photocatalytic processes.

Mohanty and co-workers fabricated Ag/ZnO/g-CN heterojunction through a novel coprecipitation method for the photodegradation of MG and RhB dye under sunlight irradiation (Mohanty *et al.*, 2021). Fig. 7a demonstrated the spherical grain morphology and Fig. 7(b-c) showed UV-vis spectra and a 2.25 eV band gap of fabricated heterojunction. Fabricated composite Ag/ZnO/g-CN demonstrated the highest photodegradation efficacy against RhB, MG, and Phenol around 97%, 91%, and 91% within 30 min under sunlight irradiation than pure g-CN and bare ZnO. Fig. 7d demonstrated the possible mechanism of photodegradation of dye using Ag/ZnO/g-CN heterojunction.

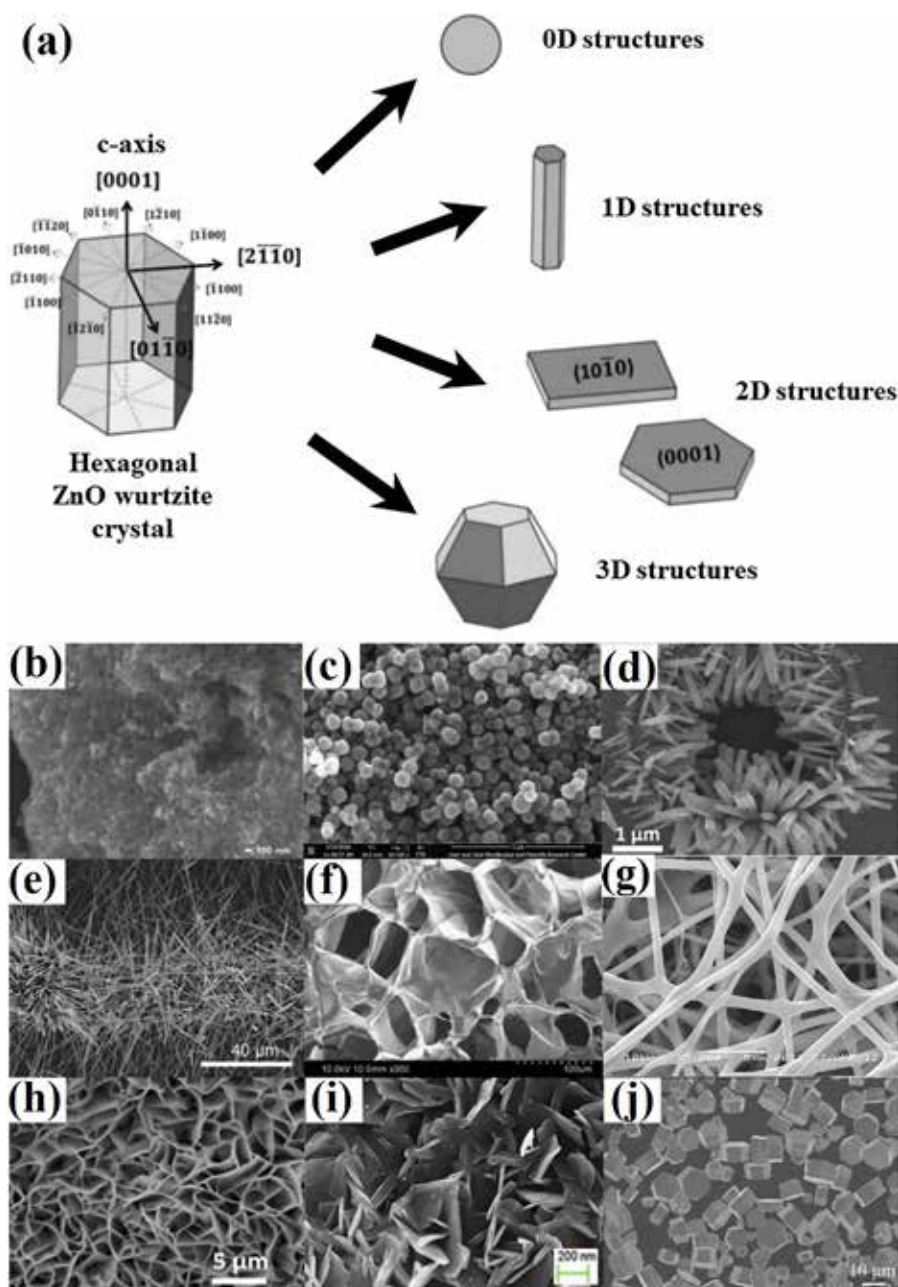


Figure 6. (a) Directions and possible shapes for crystal formation in ZnO wurtzite open access (Leonardi, 2017), complicated ZnO morphologies with a wide range of measurements: (b) quantum dots, (c) nanospheres are 0D ZnO, Adapted with permission from Elsevier (License No. 5583650527081, 5583650296604) (Saleh, 2019; Sun *et al.*, 2020). (d) nanorods (Lee *et al.*, 2020), (e) nanowires, Adapted with permission from Elsevier (License No. 5583651015432) (Kong *et al.*, 2018), (f) nanobelts, Adapted with permission from Elsevier (License No. 5583761288257) (Rao *et al.*, 2019), and (g) nanofibers, Adapted with permission from Elsevier (License No. 501830453) (Imran *et al.*, 2017) are all 1D ZnO structures. (h) nanosheets, Adapted with permission from Elsevier (License No. 5583770341756) (Manjula *et al.*, 2020), (i) nanoflakes, Adapted with permission from Elsevier (License No. 5583770192935) (Arasu *et al.*, 2019), and (j) disk-like, Adapted with permission from Elsevier (License No. 5583770622534) (Zhu, Q. *et al.*, 2018) structures made of 2D ZnO.

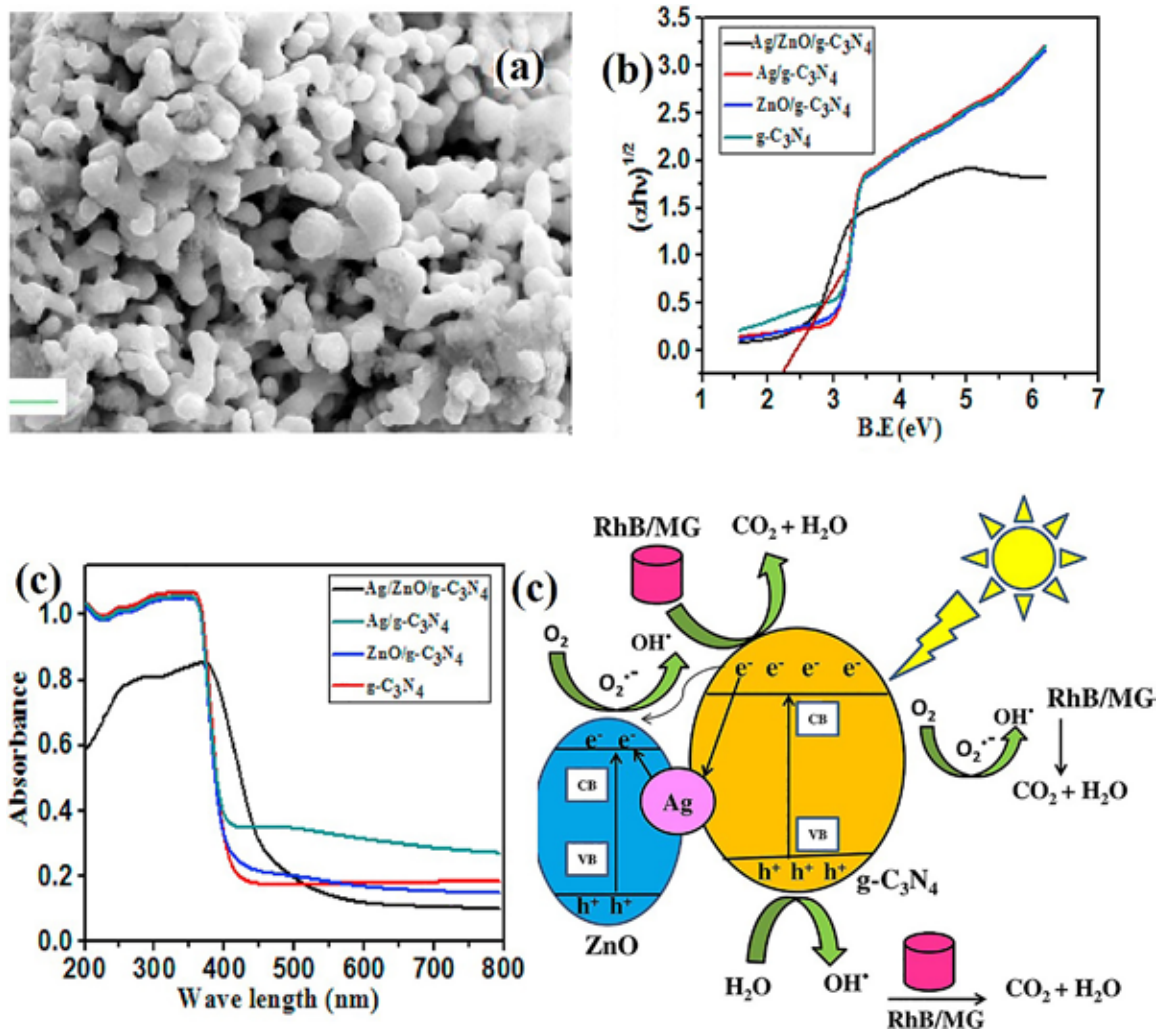


Figure 7. (a) SEM image of fabricated heterojunction, (b) UV-visible spectra, (c) Tauc plot of fabricated nanoparticles, (d) Schematic representation of photodegradation of RhB and MG dye through Ag/ZnO/g-CN, Adapted with permission from Elsevier (License No. 5583781503399) (Mohanty *et al.*, 2021).

He and colleagues fabricated g-CN/ZnO nanocomposite through the simple solid-state process for the conversion of CO₂ to fuels (He *et al.*, 2015). g-CN/ZnO composite demonstrated aggregation of wrinkled sheets-like morphology as shown in Fig. 8a and band gap around 2.63eV as shown in Fig. 8b. The highest CO₂ conversion rate was observed for the ZnO/g-CN photocatalyst around 45.6 $\mu\text{mol h}^{-1}\text{gcat}^{-1}$. When matched to ZnO and g-CN, the CO₂ conversion rate of the optimum ZnO/g-CN photocatalyst was 4.9 and 6.4 times higher, respectively as shown in Fig. 8c. Using a ZnO/g-CN heterojunction, a potential process for converting CO₂ into fuels was shown in Fig. 8d.

4. MODIFICATION STRATEGIES TO ENHANCE PHOTOCATALYTIC EFFICIENCY OF g-CN-based ZnO PHOTOCATALYSTS

Currently, ZnO and g-CN photocatalysts have been extensively studied to get rid of increasing water pollution (Paul *et al.*, 2020). However, pristine ZnO and g-CN showed rapid e⁻/h⁺ pair recombination effect that limits their photocatalytic applications (Kong *et al.*, 2017). Fabrication of g-CN-based ZnO-photocatalysts via heterojunction construction such as type-II heterojunction, Z-scheme, and S-scheme has been regarded as a notable approach to improve the charge separation, meanwhile, enhancing the photocatalytic activity.

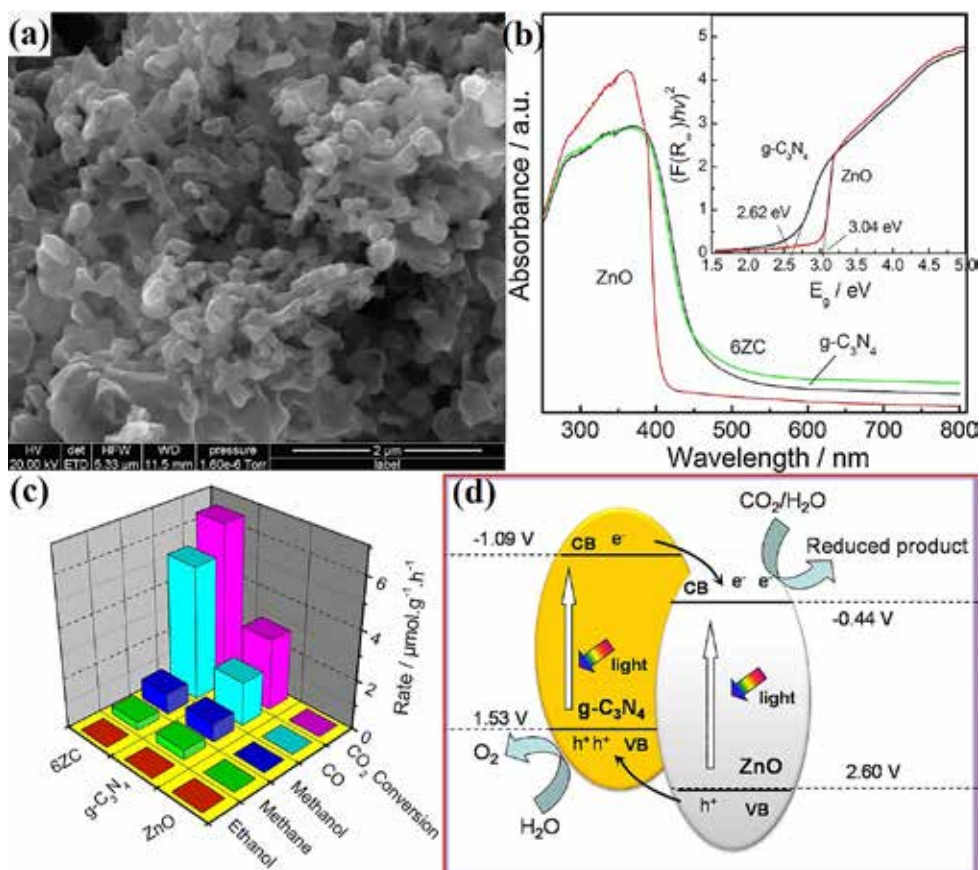


Figure 8. (a) SEM image, (b) UV-visible spectra of fabricated g-CN/ZnO nanocomposite, (c) Photocatalytic efficacy of conversion CO_2 into fuels, (d) Schematic representation of photocatalytic conversion of CO_2 into fuels using fabricated g-CN/ZnO nanocomposite, Adapted with permission from Elsevier (License No. 5583790376862) (He *et al.*, 2015).

4.1. Type-II heterojunction

The photocatalysts showed potent redox ability to produce ROS for effective photodegradation using a wide range of visible light. However, pristine photocatalysts are unable to achieve the required potentials because narrow band gaps use a broad spectrum of visible light and anticipated rapid e^- - h^+ recombination (Low *et al.*, 2017). Researchers have reported that heterojunction formation between various photocatalysts proficiently suppresses the e^- - h^+ recombination due to differences in their VB and CB potentials. Based on band alignments conventional heterojunctions are categorized as type-I, type-II, and type-III (Low *et al.*, 2017). Out of these, the charge migration pathway in type-II (staggered gap) heterojunction is more effective than type-I (straddling gap) and type-III (broken gap) heterojunction (Dhull *et al.*, 2023). The photo-induced e^- in type-II heterojunction gets migrated to the

reduction potential of SC-I and h^+ to the oxidation potential of SC-II resulting in enhanced photocatalytic activity. For the degradation of MB, Jang *et al.* fabricated a g-CN@ZnO heterojunction via atomic layer deposition (ALD) (Jang *et al.*, 2019). By ALD of ZnO on g-CN, observed PL intensity was low indicating that the formed heterostructure between g-CN and ZnO (GZ5) impeded the e^- - h^+ pair recombination effectively and enhanced the photoactivity Fig. 9(a). From their experiments, it was observed that out of as-prepared samples, the GZ5 showed up to 96.4% degradation of MB under optimal conditions. Considering the mechanism from Fig. 9(c), the g-CN e^- from the LUMO was migrated to the CB of ZnO, leaving g-CN h^+ in HOMO. The LUMO of g-CN (-1.1 eV) is more negative than the CB of ZnO (-0.27). Therefore, because of this effective charge separation, the e^- / h^+ pair recombination was suppressed, which ultimately increases the photoactivity of g-CN@ZnO composites.

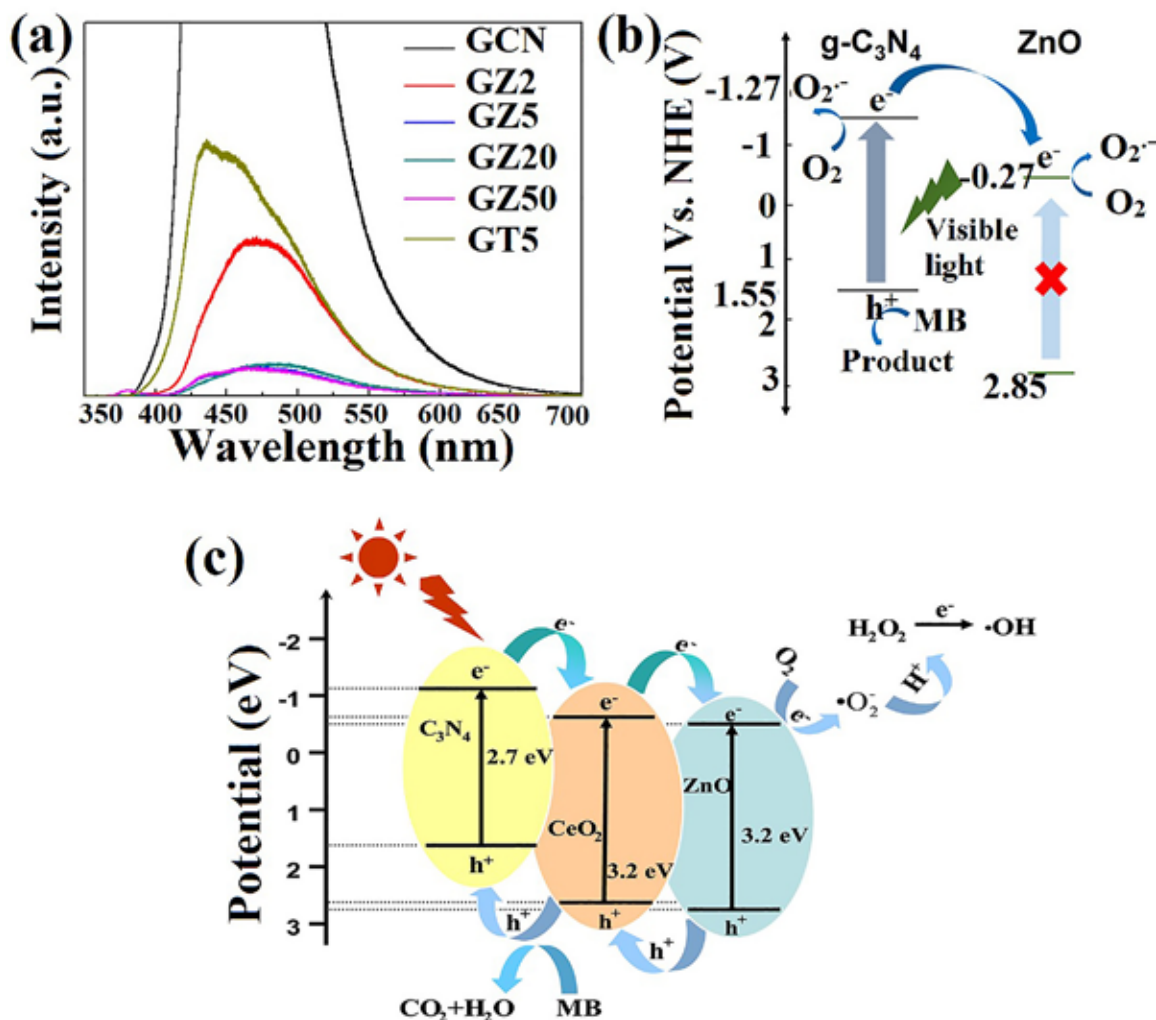


Figure 9. (a) PL intensity of the as-prepared samples GCN, GZ2, GZ5, GZ20, GZ50 and GT5, (b) Schematic representation of the mechanism of g-CN@ZnO composite, Adapted with permission from Elsevier (License No. 5517790468280) (Jang *et al.*, 2019). (c) Illustrated mechanism of the type-II g-CN/CeO₂/ZnO ternary nanocomposites, Adapted with permission from Elsevier (License No. 5517790623801) (Yuan *et al.*, 2017).

Similarly, Huang *et al.* successfully synthesized g-CN/CeO₂/ZnO ternary nanocomposites that degraded MB when exposed to UV-visible light irradiation (Yuan *et al.*, 2017). From the reported work, it was inferred that the resultant type-II band position with effective migration of excited e⁻-h⁺ in g-CN/CeO₂/ZnO nanocomposite was responsible for improved photo-induced charge separation. From the mechanism Fig. 9(c), it was noted that E_{CB} of g-CN was more than E_{CB} ZnO and CeO₂, e⁻ in the CB of g-CN were moved to CB of CeO₂ and CB of ZnO under the effect of an inner electric field between them. Meanwhile, h⁺ in the VB of ZnO was migrated to the VB of CeO₂ and the VB of g-CN. Since the fabricated g-CN/CeO₂/ZnO nanocomposites had

complementary band potentials, photocatalytic activity for organic pollutant destruction was significantly improved.

4.2. Z-Scheme heterojunction

In recent years, the Z-scheme heterojunction has received a lot of attention for its remarkable potential in various applications. Z-scheme heterojunctions when compared with type-II heterojunctions, exhibit enhanced charge separation, and transfer due to the staggered energy band alignment, leading to the improved redox ability of photocatalysts. In this regard, Wang *et al.* prepared Oxygen defects-mediated g-CN/ZnO Z-scheme

heterojunction for the removal of 4-chlorophenol and hydrogen production (Wang, J. *et al.*, 2017). The PL spectra results showed that the CN-10/OD-ZnO heterostructure impeded the recombination of the e^-h^+ pair effectively Fig. 10(a). This was also confirmed through the EIS spectra and the CN-10/OD-ZnO exhibited almost 95% degradation of 4-CP within 60 min of irradiation Fig. 10(b). Considering mechanism Fig. 10(d), the trapped electrons of OD-ZnO recombined with the VB h^+ of g-CN, resulting in the accumulation of photogenerated CB e^- of g-CN and VB h^+ of ZnO. Thereby, oxygen vacancies in OD-ZnO help in improving the absorption of light and facilitating the effective charge migration of the g-CN/OD-ZnO composite, resulting in improved photocatalytic removal of 4-chlorophenol. Moreover, the CN-10/OD-ZnO composite demonstrated an excellent visible-light

Z-scheme evolution rate of H_2 , approximately five times that of pristine g-CN Fig. 10(c). A Z-scheme g-CN/ZnO/NiFe₂O₄ heterojunction for photocatalytic removal of fluoroquinolone (FQs) antibiotics prepared by Garg *et al.* (Garg *et al.*, 2022). To examine the e^-h^+ recombination rate, PL and EIS spectra were observed for as prepared samples (CN, ZnO, NiFe₂O₄, CZN1, CZN2, and CZN3), the CZN1 showed the highest efficacy of photo-induced charge carriers' separation. This could be attributed to the double charge transfer pathways established in the heterostructure, as this provided a dual Z-scheme mechanism that inhibited the recombination of the photo-induced electron-hole pairs. Therefore, the ternary heterostructure CZN1 demonstrated an enhanced photocatalytic performance and showed a 94% degradation rate of FQs antibiotics within 90 min

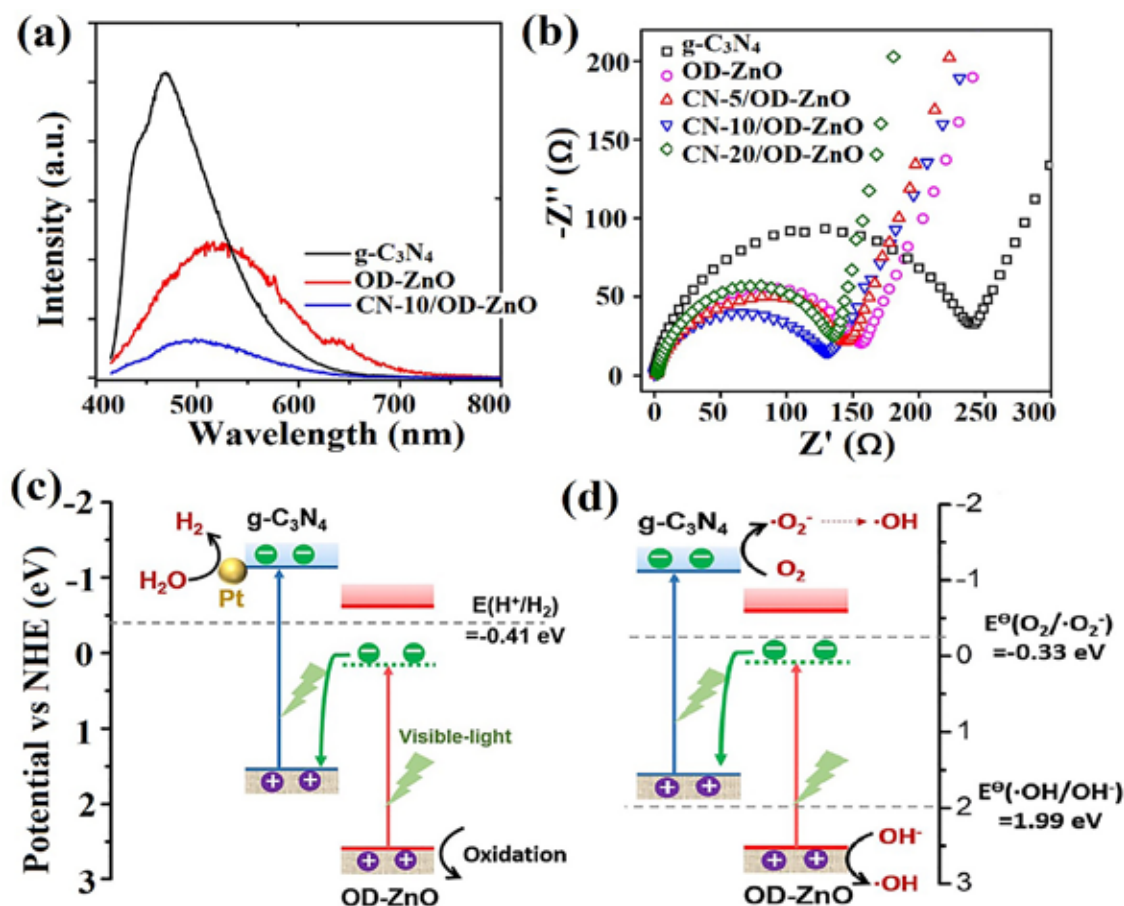


Figure 10. (a) PL intensity of the sample g-CN, OD-ZnO and CN-10/OD-ZnO, (b) EIS spectra of the samples, g-CN, OD-ZnO, CN-5/OD-ZnO, CN-10/OD-ZnO and CN-20/OD-ZnO (c) Schematic representation of the photocatalytic H₂ production through Z-scheme g-CN@ZnO composite, (d) Illustration of the Z-scheme for pollutant degradation, Adapted with permission from Elsevier (License No. 5517770955621) (Wang, J. *et al.*, 2017).

4.3. S-scheme heterojunction

S-scheme is a rational charge transfer mechanism that showed efficient charge separation and migration due to internal electric field and band bending as compared to type-II and Z-scheme heterojunctions. In an S-scheme heterojunction, two semiconductors form an interface in such a way, that an e⁻ depletion layer and an e⁻ accumulation layer are formed between the positively charged reduction photocatalyst (RP) and negatively charged oxidation photocatalyst (OP). This promoted band bending as the fermi energy is at the same level. Consequently, the photo-induced CB e⁻ of OP and VB h⁺ of RP tend to recombine at the interface region, and eventually, the VB of OP and CB of RP, which have strong redox abilities, are formed (Zhang, L. *et al.*, 2022). In this regard, S-scheme g-CN/ZnO heterojunction was synthesized for the degradation of azo dye (Lee *et al.*, 2022). For their experimental work, they prepared various samples using ZnO as a precursor and Zeolitic-imidazolate-framework-8 (ZIF8) as a template of g-CN. Out of as prepared samples, CN/ZIF8-450 displayed the best photodegradation results (95%), which was 1.6 times greater than pure CN (43%), within 1h. Due to its high specific surface area (182.8 m²/g), which is 3.4 times greater than CN (536 m²/g), and its recombination rate reduced, the CN/ZIF8-450 heterojunction exhibited excellent performance.

In another study, an S-scheme 2D/2D N-ZnO/CN heterojunction was fabricated for the degradation of fluoroquinolone antibiotics. Various samples with different mass ratios (ZIF-L/CN) of 5%, 10%, 15%, and 20% were prepared by Zhang *et al.* (Zhang, C. *et al.*, 2022). According to the findings, 15% NZCN showed lower PL spectra, indicating more effective separation of charge carriers Fig. 11a. The EIS spectra further demonstrated that the 15% NZCN showed a smaller arc radius, suggesting higher photogenerated charge transferability Fig. 11b. From, the S-scheme photocatalytic mechanism shown in Fig. 11c, CB e⁻ of N-ZnO were transferred to the VB of CN and combined with h⁺. The VB h⁺ of N-ZnO reacts with OH⁻ to produce ·OH radicals, and CB e⁻ of CN combined with O₂ to give ·O₂⁻. Furthermore, the combination of ·O₂⁻ and h⁺ results in the formation of ¹O₂. Finally, the ROS, namely ·O₂⁻, ·OH, and ¹O₂, along with h⁺, have been observed to exhibit significant efficacy in the photodegradation of fluoroquinolone antibiotics (FQs). Using 15% NZCN heterojunction, the degradation efficiency

of NOR, ENR, LVF, and CIP could exceed 90% in 90 minutes. Similarly, another heterojunction photocatalyst g-CN/Co/ZnO has been reported for the removal of dye (Leelavathi *et al.*, 2023). In terms of optoelectronic properties, it was observed that the g-CN/Co/ZnO composite exhibited excellent photocatalytic performance, as the Co and ZnO had an impact on the band gap energy, photo-induced e⁻-h⁺ pair separation as well as decreased the charge migration resistance which resulted in enhanced degradation ability. The authors used MB, CV, and RhB cationic dyes as target pollutants to evaluate the photocatalytic efficacy of g-CN/Co/ZnO photocatalysts. The attained removal efficiencies of the MB, CV, and RhB dyes were 96.3%, 74.5%, and 75.14%, respectively.

5. APPLICATIONS OF g-CN/ZnO-based NANOCOMPOSITE FOR POLLUTANT DEGRADATION AND ENERGY CONVERSION

5.1. Pollutant degradation

Zhang and co-workers fabricated g-CN/ZnO@graphene heterojunction through the facile hydrothermal self-assemble process for the photodegradation of RhB dye within 120 min under visible light irradiation (Zhang, J.-Y. *et al.*, 2019). g-CN/ZnO@graphene (30%) photocatalyst demonstrated maximum RhB photodegradation efficiency of around 82.7% and 81% under sunlight and UV light respectively within 120 minutes. Fabricated g-CN/ZnO@graphene (30%) photocatalyst showed S-scheme possible mechanism for the RhB degradation (Fig. 12a). Hashem *et al.*, designed CdS@ZnO/g-CN heterojunction through novel ultrasonication assisted process for the elimination of RhB within 180 min (Hashem *et al.*, 2021). Fabricated CdS@ZnO/g-CN heterojunction photo degraded RhB dye completely within 2hr and 3hrs under UV-light and visible irradiation respectively. CdS@ZnO/g-CN photocatalyst demonstrates Z-scheme/type II heterojunction mechanism for the photodegradation RhB dye as shown in Fig. 12b. Bahiraei and colleague's synthesized magnetic CoFe₂O₄/g-CN/ZnO nanocomposite through in-situ chemical precipitation process for MB photodegradation (Bahiraei *et al.*, 2023). CoFe₂O₄/g-CN/ZnO nanocomposite photo degraded around 92% MB dye within 100 min light irradiation. While bare CoFe₂O₄/g-CN and CoFe₂O₄/ZnO degraded MB dye around

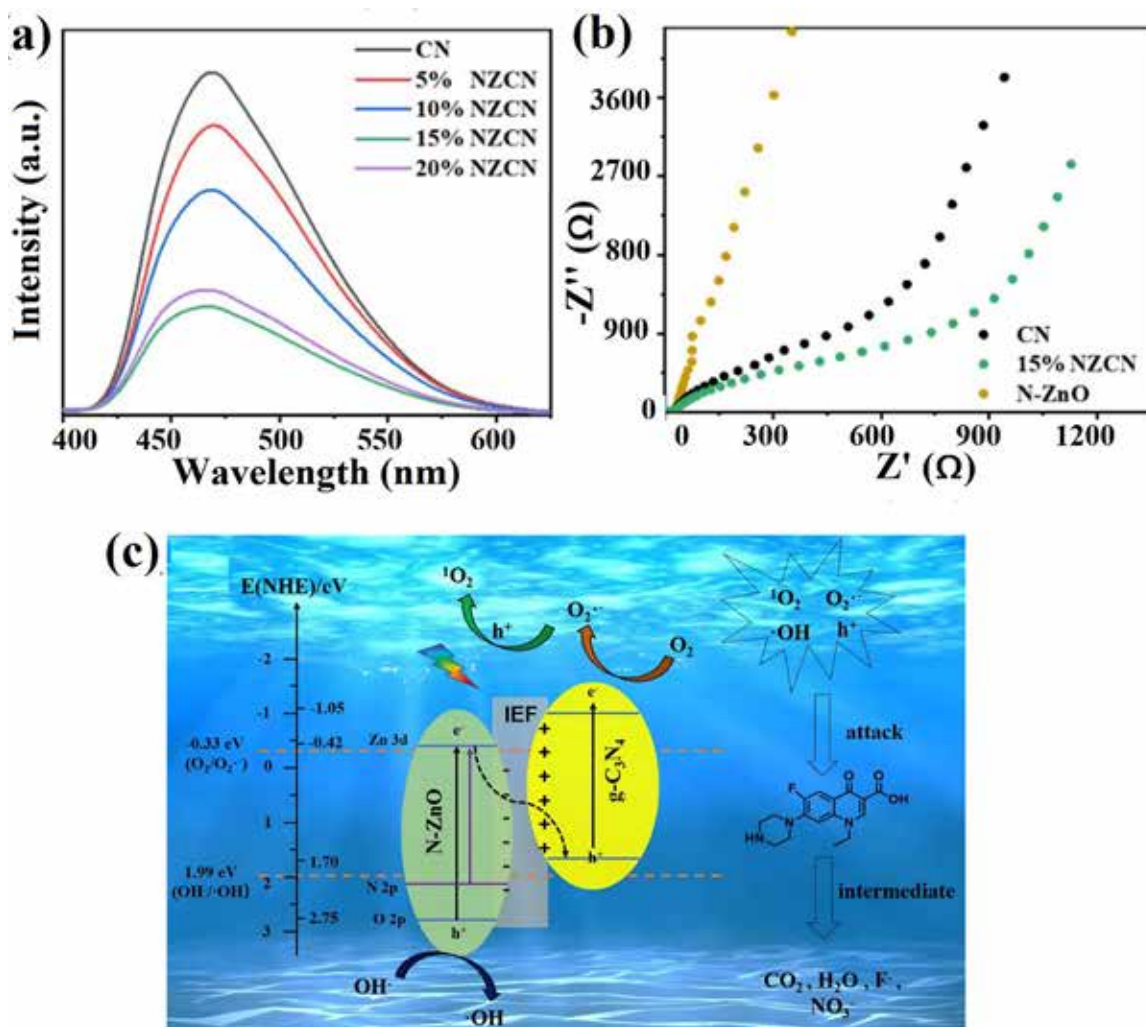


Figure 11. (a) PL intensity of the samples CN, 5% NZCN, 10% NZCN, 15% NZCN and 20% NZCN, (b) EIS spectra of the as-prepared samples, (c) Schematic representation of S-scheme mechanism of 2D/2D N-ZnO/CN heterojunction, Adapted with permission from Elsevier (License No. 5517710737286) (Zhang, C. *et al.*, 2022).

49% and 31% respectively. Magnetic $CoFe_2O_4$ /g-CN/ZnO photocatalyst followed the type II heterojunction mechanism for the photodegradation of MB dye under visible light irradiation. Similarly, $Ag/Ag_2O@ZnO@g-CN$ nanocomposite was designed through the novel hydrothermal process for the photodegradation of MB dye under visible light irradiation (Wang, 2023). MB was completely degraded by fabricated $Ag/Ag_2O@ZnO@g-CN$ nanocomposite within 50 min under visible light irradiation while $Ag/Ag_2O@g-CN$, $ZnO@g-CN$, and bare g-CN demonstrates 91.611%, 87.724%, and 64.48% degradation of MB dye. Fabricated $Ag/Ag_2O@ZnO@g-CN$ nanocomposite showed p-n type heterojunction for the degradation of MB dye.

Thuan *et al.* fabricated ZnO-modified g-CN nanoparticles through the facile hydrothermal process for the photodegradation of ciprofloxacin within 120 min under sunlight irradiation (Van Thuan *et al.*, 2022). Ciprofloxacin photodegradation reached around 93.8% by g-CN/ZnO within 120 min at pH 8.0 and the ciprofloxacin photodegradation rate for g-CN/ZnO photocatalyst was 4.9 times faster than bare g-CN as demonstrated in Fig. 13a. Designed g-CN/ZnO photocatalyst followed type mechanism for the degradation of ciprofloxacin as shown in Fig. 13b. Furthermore, Pham *et al.*, designed ZnO/g-CN photocatalyst for photodegradation of tetracycline within 60 min under sunlight (Pham *et al.*, 2023). Fabricated ZnO/g-CN photocatalyst degraded

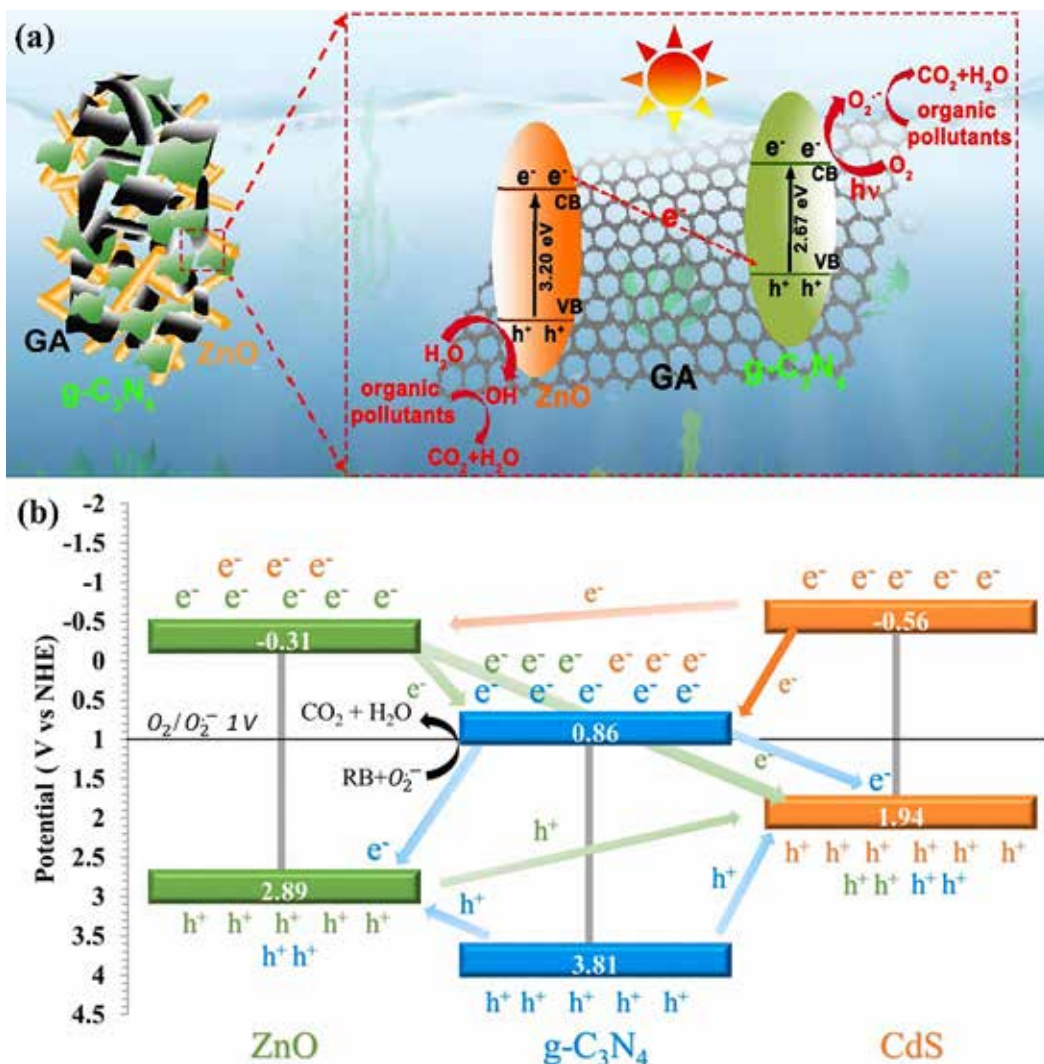


Figure 12. Schematic illustration of photodegradation of dye using (a) ZnO/g-CN@graphene photocatalyst, Adapted with permission from Elsevier (License No. 5583791082817) (Zhang, J.-Y. *et al.*, 2019), (b) CdS@ZnO/g-CN heterojunction, Adapted with permission from Elsevier (License No. 5583790844106) (Hashem *et al.*, 2021).

tetracycline around 92.6% within 60 min under light irradiation as shown in Fig. 13c and tetracycline photodegradation rate was 5 times more by ZnO/g-CN photocatalyst than bare g-CN nanocomposite. Fabricated ZnO/g-CN photocatalyst follows type II heterojunction mechanism for the photodegradation of tetracycline as shown in Fig. 13d. Similarly, chi and co-workers synthesized ZnO/g-CN nanocomposite through novel deposition-precipitation process for the degradation of tetracycline hydrochloride under visible light irradiation (Chi *et al.*, 2022). Maximum tetracycline hydrochloride was photo degraded by ZnO/g-CN nanocomposite around 100%, while bare g-CN and ZnO nanoparticles degraded around

88%, and 65% within 45 min under sunlight. Correspondingly, Zhu *et al.*, fabricated ZnO/Cu₂O₄/g-CN heterojunction by a facile one-pot synthesis process for the photodegradation of chlortetracycline, tetracycline, ciprofloxacin, and oxytetracycline within 120 min (Zhu, Y. *et al.*, 2022). Fabricated ZnO/Cu₂O₄/g-CN showed photodegradation efficiency around 99.5%, 98.79%, 95.35%, and 73.53% respectively within 120 min under visible light irradiation. ZnO/Cu₂O/g-CN photocatalysts degraded TC at a rate 10.62 and 1.35 times greater than g-CN and Cu₂O/g-CN, respectively, in the first 30 min ZnO/Cu₂O₄/g-CN demonstrates p-n-n type mechanism for the photodegradation of these antibiotics.

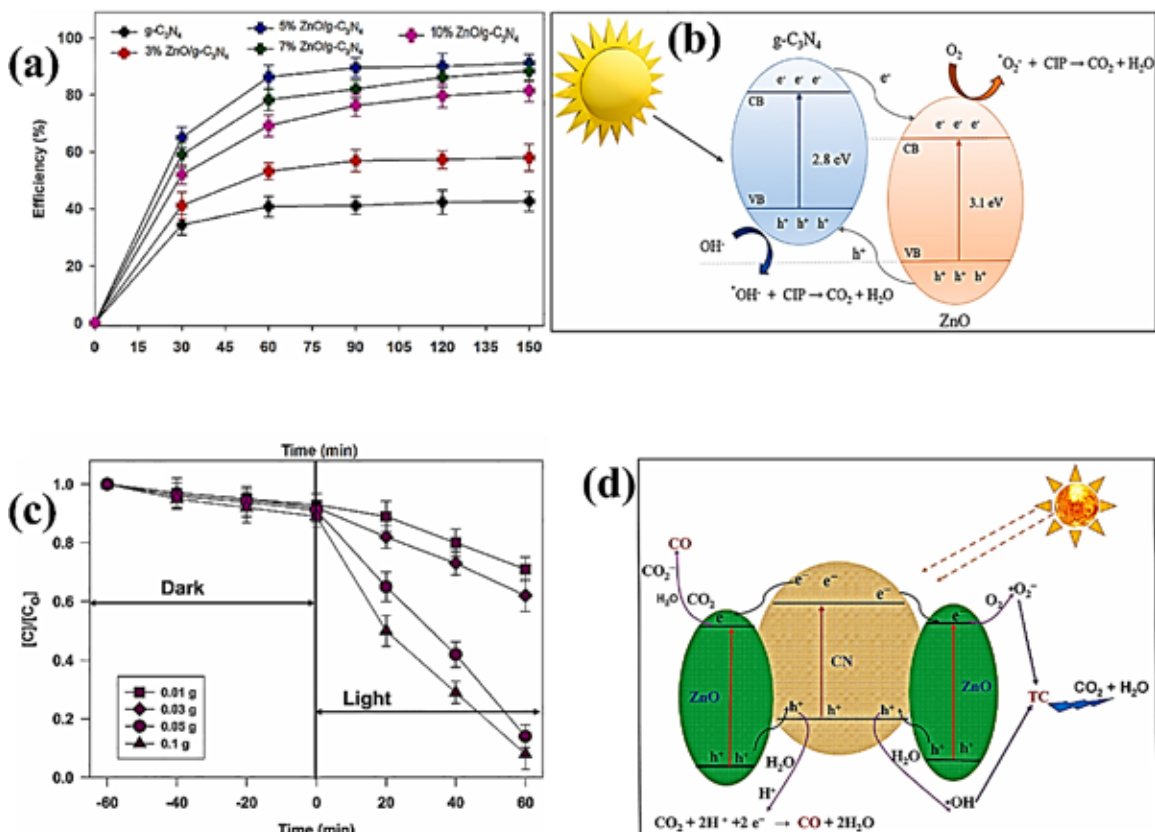


Figure 13. (a) Photodegradation of ciprofloxacin using ZnO/g-CN photocatalyst, (b) Schematic illustration of ZnO/g-CN photocatalyst for ciprofloxacin photodegradation, Adapted with permission from Elsevier (License No. 5583791393112) (Van Thuan *et al.*, 2022), (c) Photodegradation of tetracycline by ZnO/g-CN photocatalyst, and (d) Schematic illustration of ZnO/g-CN photocatalyst for tetracycline photodegradation, Adapted with permission from Elsevier (License No. 5583800040586) (Pham *et al.*, 2023).

5.2. Hydrogen production

Liu and colleagues synthesized g-CN/ZnO type II heterojunction nanorods through a facile light-assisted method for the photocatalytic efficiency of hydrogen production (Liu, J. *et al.*, 2020). The formation of such a type of heterojunction promotes charge separation and increases the interfacial charge transfer (Fig. 14a). g-CN/ZnO-3 nanorods demonstrated around 23 μmol of hydrogen amount produced within 3h as shown in Fig. 14b. In particular, g-CN/ZnO heterostructure enhanced photocatalytic hydrogen production by 3.3 times than ZnO NRAs with 85% retention rate stability after 5 cycles. Similarly, nitrogen-doped g-CN/ZnO Z-scheme heterojunctions have been designed through the novel process for hydrogen evolution by Liu and co-workers (Fig. 14c) (Liu, X. *et al.*, 2020). N doped ZnOCN1 composite showed a high

hydrogen production rate was around 0.78 mmol g⁻¹h⁻¹, which is 77% more than bare g-CN as shown in Fig. 14d. Similarly, g-CN/ZnO/Au photocatalyst was fabricated by Ge and coworkers through simple chemical method for the photocatalytic hydrogen production (Ge *et al.*, 2023). g-CN/ZnO/Au photocatalyst hydrogen production rate was around 46.46 μmol g⁻¹h⁻¹, while bare g-CN and g-CN/ZnO demonstrated around 1.59 μmol g⁻¹h⁻¹ and 1.843 μmol g⁻¹h⁻¹ respectively.

5.3. CO₂ reduction

Li and coworkers synthesized g-CN/ZnO nanoparticles decorated with Ti₃C₂ through a facile coprecipitation process for the photocatalytic reduction of CO₂ (Li *et al.*, 2023). In this work, g-CN/ZnO/Ti₃C₂ demonstrated around 6.41 μmol g⁻¹h⁻¹ CO production while bare g-CN, ZnO, and g-CN/ZnO showed

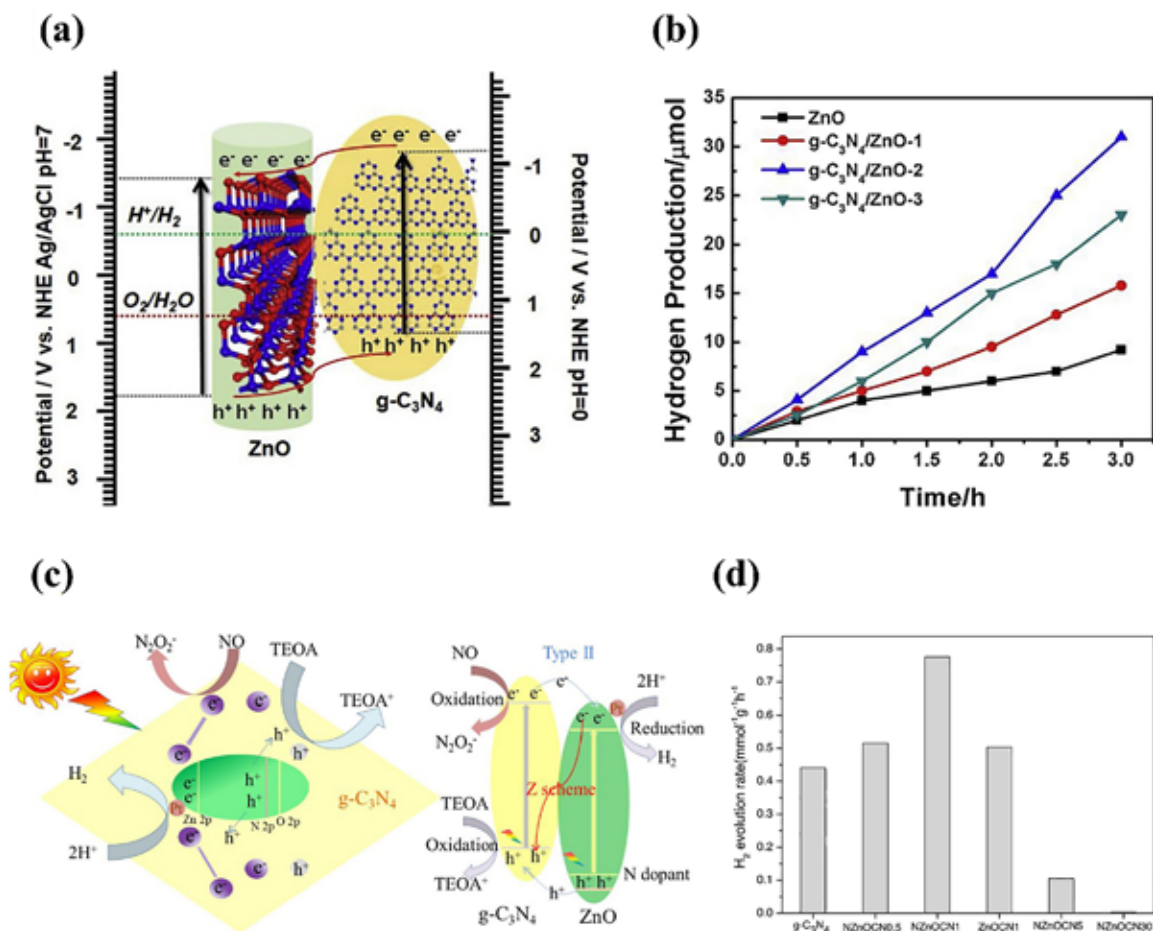


Figure 14. (a) Schematic mechanism of ZnO-g-CN nanocomposite, (b) hydrogen evolution by fabricated photocatalysts, Adapted with permission from Elsevier (License No. 5584071333686) (Liu, J. *et al.*, 2020), (c) Schematic illustration of Nitrogen rich g-CN/ZnO photocatalyst, and (d) rate of hydrogen evolution by synthesized nanocomposites, Adapted with permission from Elsevier (License No. 5584080008309) (Liu, X. *et al.*, 2020).

only 0.79 $\mu\text{mol g}^{-1}\text{h}^{-1}$, 0.52 $\mu\text{mol g}^{-1}\text{h}^{-1}$, 1.41 $\mu\text{mol g}^{-1}\text{h}^{-1}$ production of CO respectively (Fig. 15a). Fabricated g-CN/ZnO/Ti₃C₂ photocatalyst follows type-II heterojunction mechanism for the reduction of CO₂ (Fig. 15b). Arif *et al.* designed ZnO/g-CN heterojunction modified with Ag through facile hydrothermal process for CO₂ reduction (Arif *et al.*, 2022). ZnO/g-CN/Ag heterojunction demonstrated production of CO and CH₄ around 36 $\mu\text{mol g}^{-1}\text{h}^{-1}$ and 14 $\mu\text{mol g}^{-1}\text{h}^{-1}$ respectively, while g-CN produced CO and CH₄ 2 $\mu\text{mol g}^{-1}\text{h}^{-1}$ and 4 $\mu\text{mol g}^{-1}\text{h}^{-1}$ (Fig. 15c). Designed Ag modified ZnO/g-CN nanocomposite showed type II heterojunction mechanism for CO₂ photoreduction. Similarly, g-CN/ZnO/graphene was fabricated through a novel process for the photo reduction of CO₂ (Wang *et al.*, 2022). CO₂ conversion rate into CO was around 33.87

$\mu\text{mol g}^{-1}\text{h}^{-1}$ using g-CN/ZnO/graphene photocatalyst, while bare g-CN demonstrated 1.61 $\mu\text{mol g}^{-1}\text{h}^{-1}$ (Fig. 15d). g-CN/ZnO/graphene photocatalyst showed an S-scheme mechanism for the reduction of CO₂. Data on different characterization techniques that can be employed to validate the properties of photocatalytic materials used in the treatment/degradation of wastewater concerning g-CN/ZnO composite is given in tabulated form in Table 2. Therefore, based on the above discussion on photocatalytic application, it can be concluded that both g-CN and ZnO-based heterojunctions have shown outstanding photodegradation ability. Furthermore, there are several patent information available related to g-C₃N₄-based photocatalysts showing good photodegradation ability towards various pollutants (Raizada).

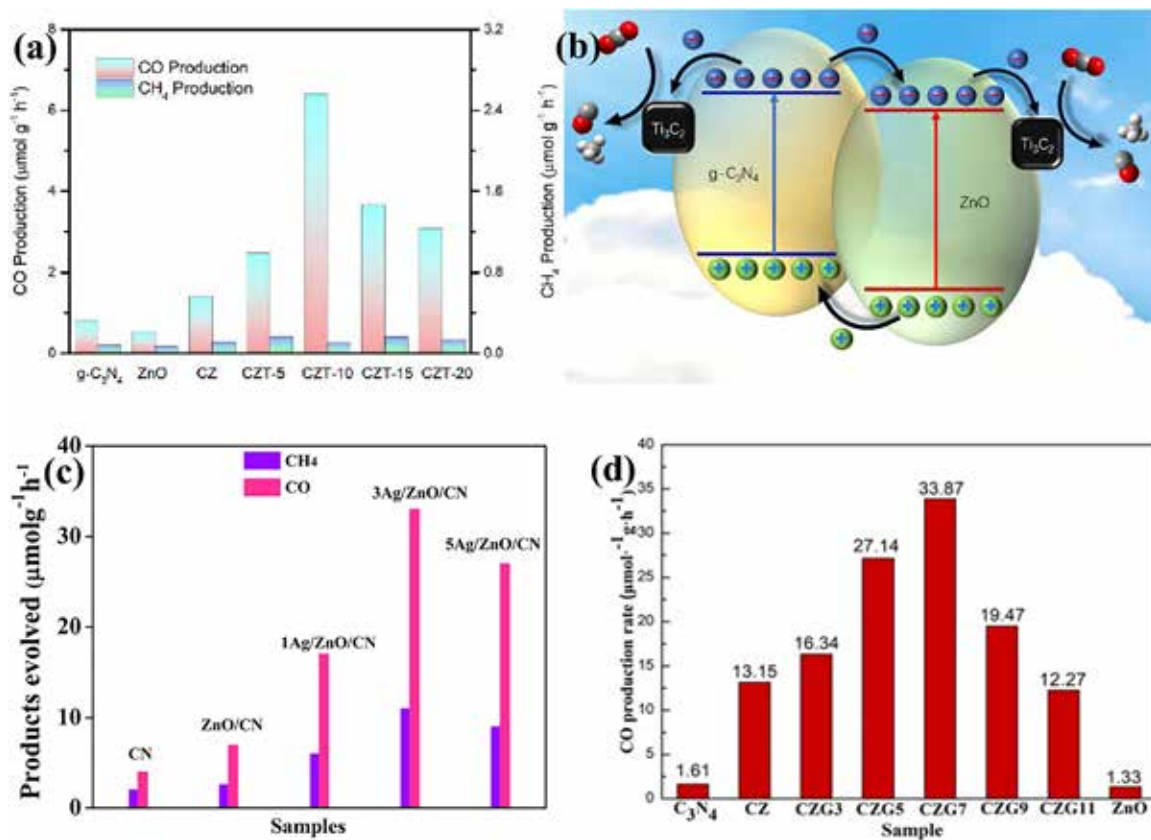
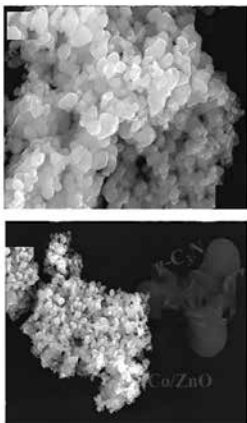
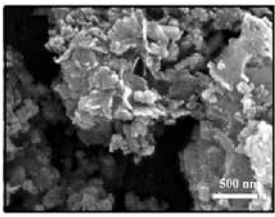
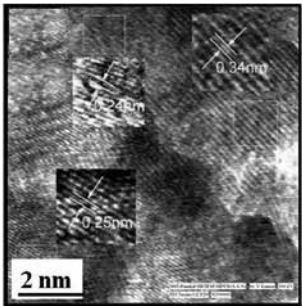
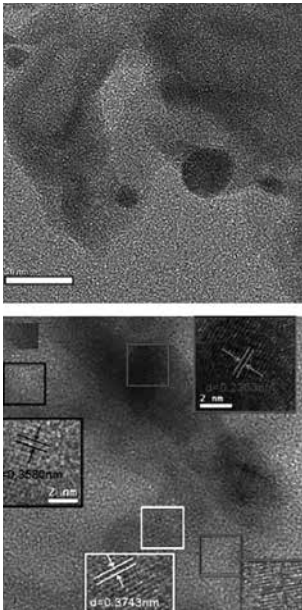
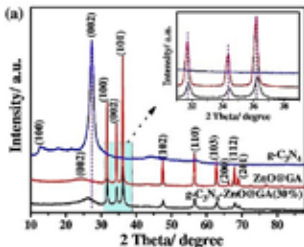
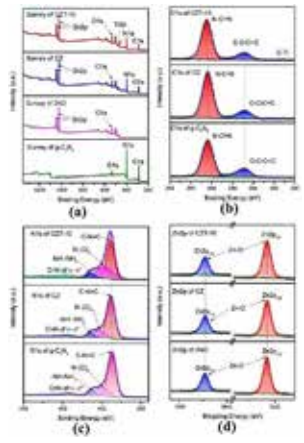
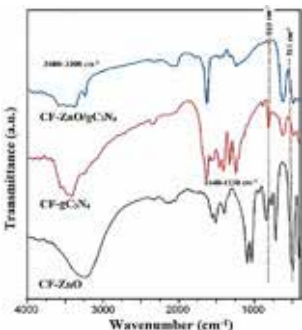
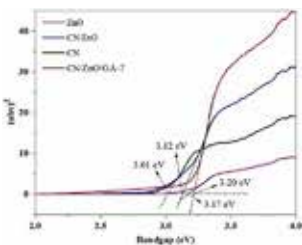
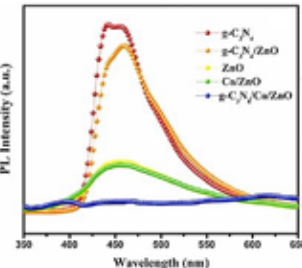


Figure 15. (a) Production of CO and CH₄, (b) Schematic mechanism of CO₂ reduction, Adapted with permission from Elsevier (Open Access) (Li *et al.*, 2023). Production rate of (c) CO and CH₄, Adapted with permission from Elsevier (License No. 5584071085210) (Arif *et al.*, 2022), and (d) CO, Adapted with permission from Elsevier (License No. 5584061422959) (Wang *et al.*, 2022).

S. No.	Characteristics	Photocatalysts	Characterization	Analysis of characterization
1	Morphological characteristics	g-C ₃ N ₄ /Co/ZnO	<p>1. SEM</p>  <p>SEM images of g-C₃N₄/Co/ZnO composite. (License no. 5660030503095) (Leelavathi <i>et al.</i>, 2023)</p>	<ul style="list-style-type: none"> SEM analysis explores the surface and morphological characteristics of the photocatalysts. On analysis, SEM images revealed a soft layered sheet-like structure of ternary composite g-C₃N₄/Co/ZnO

S. No.	Characteristics	Photocatalysts	Characterization	Analysis of characterization
1	Morphological characteristics	CoFe ₂ O ₄ /g-C ₃ N ₄ /ZnO	 <p>SEM image of CoFe₂O₄/g-C₃N₄/ZnO nanocomposite. (License no. 5660040185077) (Bahiraei <i>et al.</i>, 2023)</p>	<ul style="list-style-type: none"> The CoFe₂O₄/g-C₃N₄/ZnO nanocomposite's SEM study revealed fine, granular, flake-like particles
		g-C ₃ N ₄ /ZnO/NiFe ₂ O ₄	 <p>High-resolution TEM image of g-C₃N₄, ZnO, NiFe₂O₄ (License no. 5660110583516) (Garg <i>et al.</i>, 2022)</p>	<ul style="list-style-type: none"> Using HR-TEM, the precise surface morphology and crystallinity of the synthesized material g-C₃N₄/ZnO/NiFe₂O₄ were explained. High-resolution TEM images show the lattice fringe widths of 0.24, 0.25, and 0.34 nm, respectively, which were consistent with XRD measurements and could be indexed to the (101), (311), and (0 0 2) plane of ZnO, NiFe₂O₄, and g-C₃N₄, respectively
		Ag/Ag ₂ O@ZnO	 <p>High-resolution TEM images of Ag/Ag₂O@ZnO/g-C₃N₄ (License no. 5660111487355) (Wang, 2023)</p>	<ul style="list-style-type: none"> ZnO, Ag₂O, and g-C₃N₄ nanoparticles were identified using an HRTEM image that allowed for the measurement of interplanar spacings and differentiation of the shades of lattice fringes. The ZnO nanoparticle's (1 0 0) plane relates to an interplanar spacing of 0.2363 nm, while the Ag₂O (2 0 0) plane is connected to an interplanar distance of 0.3000 nm. Additionally, the (0 0 2) facet of g-C₃N₄ corresponded to 0.3580 nm and 0.3743 between its bright fringes.

S. No.	Characteristics	Photocatalysts	Characterization	Analysis of characterization
2	Structural and chemical properties	$g\text{-C}_3\text{N}_4/\text{ZnO}/\text{Graphene Aerosol}$	<p>1. XRD (X-ray diffraction)</p>  <p>XRD patterns of several samples of $g\text{-C}_3\text{N}_4$, ZnO/Graphene Aerosol, $g\text{-C}_3\text{N}_4/\text{ZnO}/\text{Graphene Aerosol}$ 30%. (License no. 5660120911646) (Zhang, J.-Y. <i>et al.</i>, 2019)</p>	<ul style="list-style-type: none"> The crystal phase structure of the sample is characterized using XRD analysis. $g\text{-C}_3\text{N}_4$ hinders the growth of ZnO crystals, resulting in a larger ZnO crystal size (33.4 nm) in the ZnO/graphene aerosol than in the $g\text{-C}_3\text{N}_4/\text{ZnO}/\text{graphene}$ aerogel heterojunction (25.3 nm).
		$g\text{-C}_3\text{N}_4/\text{ZnO} / \text{Ti}_3\text{C}_2$	<p>2. XPS (X-ray photoelectron spectroscopy)</p>  <p>XPS spectra of C 1s, N 1s and Zn 2p for $g\text{-C}_3\text{N}_4$, ZnO, $g\text{-C}_3\text{N}_4/\text{ZnO}$ and $g\text{-C}_3\text{N}_4/\text{ZnO}/\text{Ti}_3\text{C}_2\text{-10}$. (Open access CC BY4.0) (Li <i>et al.</i>, 2023)</p>	<ul style="list-style-type: none"> XPS spectra are employed to discuss the binding energies and surface chemical states. The survey plot of the XPS spectra for $g\text{-C}_3\text{N}_4/\text{ZnO}/\text{Ti}_3\text{C}_2\text{-10}$ showed the distinct peaks of the elements Ti, Zn, O, C, and N. The high-resolution C1s spectrum of $g\text{-C}_3\text{N}_4/\text{ZnO}/\text{Ti}_3\text{C}_2\text{-10}$ where three binding energy peaks are found at 281.21, 284.80, and 288.45 eV. The N1s XPS spectrum is entirely derived from $g\text{-C}_3\text{N}_4$, which fits into four peaks at eV: 398.83, 399.59, 401.39, and 404.46. The splitting energy of the two major split-orbit components in the Zn 2p peaks is 23.10 eV.

S. No.	Characteristics	Photocatalysts	Characterization	Analysis of characterization
2	Structural and chemical properties	CoFe ₂ O ₄ /ZnO/g-C ₃ N ₄	<p>3. FTIR</p>  <p>FTIR spectra of CoFe₂O₄/ZnO, CoFe₂O₄/g-C₃N₄, CoFe₂O₄/ZnO/g-C₃N₄ (License no. 5660040185077) (Bahraei <i>et al.</i>, 2023).</p>	<ul style="list-style-type: none"> FTIR spectra of the produced CoFe₂O₄/g-C₃N₄/ZnO nanocomposites were recorded to examine their bond structures. The Zn–O stretching, which validates the formation of ZnO, is responsible for the sharp peak at 511 cm⁻¹. The peak located at 807 cm⁻¹ in the g-C₃N₄ spectrum is attributed to the absorption of triazine units. The broad absorption peak in the 3300–3600 cm⁻¹ range may be associated with adsorbed H₂O molecules or the N–H group's stretching mode
3	Optical and Electrochemical properties	CN/ZnO/Graphene aerosol	<p>1. Tauc plot</p>  <p>Band gap values of different samples of CN, ZnO, CN/ZnO, CN/ZnO/Graphene aerosol. (License no. 5660131266486) (Wang <i>et al.</i>, 2022).</p>	<ul style="list-style-type: none"> The bandgaps of CN, ZnO, CN/ZnO, and CN/ZnO/Graphene Aerosol were found to be 3.01, 3.12, 3.17, and 3.20 eV, respectively calculated using Tauc plots. Contrary to this CN showed visible light absorption < 480 nm wavelength. Due to the presence of Graphene Aerosol the CN/ZnO/Graphene Aerosol nanocomposites showed a wide range of light absorption.
		g-C ₃ N ₄ /Co/ZnO	<p>2. PL(Photoluminescence spectroscopy)</p>  <p>PL Spectra of g-C₃N₄, g-C₃N₄/ZnO, ZnO, Co/ZnO, g-C₃N₄/Co/ZnO (License No. 5660030503095) (Leelavathi <i>et al.</i>, 2023)</p>	<ul style="list-style-type: none"> Comparing g-C₃N₄/Co/ZnO ternary nanocomposites to pure g-C₃N₄ and ZnO, a notable decrease in PL emission intensity has been observed. PL implies that in the g-C₃N₄/Co/ZnO composite, metallic Co and ZnO nanoparticles serve as an effective electron-accepting material that prevents the direct recombination of electron-hole pairs and speeds up the separation of photogenerated charges

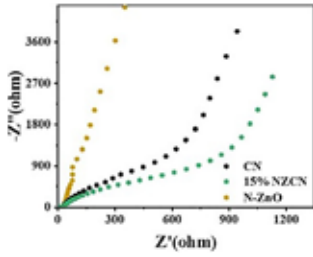
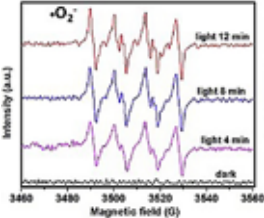
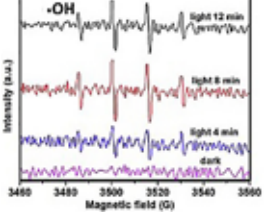
S. No.	Characteristics	Photocatalysts	Characterization	Analysis of characterization
3	Optical and Electrochemical properties	N-ZnO/g-C ₃ N ₄	<p>3. EIS (Electrochemical Impedance Spectroscopy)</p>  <p>EIS measurements of several samples of CN, 15% N-ZnO/g-C₃N₄, ZnO. (License no. 5660140267593) (Zhang, C. et al., 2022)</p> <p>EPR (Electron paramagnetic resonance)</p> 	<ul style="list-style-type: none"> EIS can likewise demonstrate how the carriers in the photocatalyst can separate and migrate. According to the EIS measurements, CN's arc radius was larger than 15% N/ZnO/g-C₃N₄, indicating that 15% N/ZnO/g-C₃N₄ had a higher photogenerated charge transferability than CN.
4	Photocatalytic properties	g-C ₃ N ₄ /ZnO	 <p>EPR spectra under dark and simulated sunlight of g-C₃N₄/ZnO nanorods. (License no. 5660551230497) (Zhong et al., 2020).</p>	<ul style="list-style-type: none"> EPR is employed for the study of unpaired electrons. In photocatalysis, the EPR technique is used to validate the generation of reactive oxygen species. The peaks of the DMPO-•OH and DMPO-•O₂⁻ signals were easily seen. The EPR intensity signal progressively rises as exposure time increases because illumination conditions result in the continuous production of •O₂⁻ and •OH radicals.

Table 2. Different characterization techniques employed to validate the properties of photocatalytic materials concerning g-CN/ZnO composite

6. CONCLUSION AND FUTURE PERSPECTIVES

Semiconductor photocatalysis as a promising technology holds potential for environmental remediation and renewable energy applications. Amongst several photocatalysts, g-C₃N₄ (g-CN) and ZnO are favorable semiconductor photocatalysts as they are cost-effective, abundant in nature, have a suitable band gap, and exhibit good stability in addition to

excellent photocatalytic properties due to which they are suitable for many environmental and energy-associated applications. The g-CN and ZnO-based photocatalysts have been broadly explored for various photocatalytic applications, including pollutant degradation, water splitting, and CO₂ reduction, making them valuable materials for sustainable energy and environmental remediation. In summary, the g-CN/ZnO-based nanocomposite represents a promising nanocomposite material

with exceptional properties and numerous potential applications. Its synthesis and characterization are critical for tailoring its properties for specific requirements. As research progresses, further advancements and optimizations of this nanocomposite will unlock its full potential, leading to breakthroughs in various fields, including energy, and environment. In the present review, we have discussed the photocatalytic properties of g-CN/ZnO-based nanocomposite towards several pollutants degradation and energy conversion with their proposed photocatalytic mechanism. We have also discussed the different modification strategies that can be employed to minimize the drawbacks of g-CN and ZnO as single photocatalysts. Through the synergistic combination of g-CN and ZnO, the formed heterojunction/nanocomposite exhibits enhanced properties that make it suitable for various photocatalytic applications. The heterojunction formation of g-CN and ZnO possesses several unique properties, such as wide or extended light absorption ability, efficient charge separation, and strong redox potential, making it highly effective in degrading organic pollutants under light irradiation. Besides, good photocatalytic properties, g-CN/ZnO nanocomposites need some exploration in their photocatalytic properties. In this conclusion, we have summarized the key findings and have discussed the future perspectives of g-C₃N₄/ZnO-based nanocomposites.

- The synthesis of g-CN/ZnO-based nanocomposites has been explored using different methods, including sol-gel, hydrothermal, and co-precipitation techniques. These methods offer flexibility in tailoring the nanocomposite's structure, morphology, and properties to suit specific applications. However, further research is needed to optimize the synthesis parameters and scale up the production of g-CN/ZnO-based nanocomposites to meet industrial demands.
- The structural, optical, and electronic properties of g-CN/ZnO-based nanocomposites play an important role in their overall performance. The intimate and strong contact between g-CN and ZnO results in improved photocatalytic activity enhanced optical and electrical properties, and superior mechanical strength. Future research should focus on understanding the underlying mechanisms governing these synergistic effects and developing advanced characterization techniques to probe the nanocomposite's structure

at the nanoscale. Also, more focus should be placed on density functional theory and theoretical calculation which will help explore their structural and electronic properties.

- One of the most promising applications of g-CN/ZnO-based nanocomposite photocatalysts lies in photocatalysis. The nanocomposite's unique properties, such as its broad absorption range, efficient charge separation, and strong redox potential, make it highly effective in degrading organic pollutants under visible light irradiation. Future studies should explore the optimization of the nanocomposite's composition, morphology, and surface properties to further enhance its photocatalytic efficiency and stability. Additionally, the development of novel reactor designs and immobilization strategies would facilitate the practical utilization of g-CN/ZnO-based nanocomposites in water and air purification systems.
- Lastly, environmental remediation is an important application area where g-CN/ZnO-based nanocomposites can play a significant role. The photoactivity of these nanocomposites can be harnessed for the removal of various wastewater pollutants (organic pollutants) and heavy metals from contaminated water and soil. Future research should focus on developing scalable and cost-effective methods for the large-scale deployment of g-CN/ZnO-based nanocomposites in real-world environmental remediation applications.

In conclusion, the g-CN/ZnO-based nanocomposites represent a versatile nanocomposite material with exceptional properties and diverse applications. Further research is needed to optimize its synthesis, understand its structure-property relationships, and explore new avenues for its application. The continued production of g-CN/ZnO-based nanocomposites will undoubtedly contribute to advancements in photocatalytic fields. ♦

REFERENCES

- ABU-SARI, S. M., ANG, B. C., DAUD, W. M. A. W., & PATAH, M. F. A. (2023). Visible-light-driven photocatalytic hydrogen production on defective, sulfur self-doped g-C₃N₄ nanofiber fabricate via electrospinning method. *Journal of Environmental Chemical Engineering*, 11(2), 109318.

- AHMAD, I., SHUKRULLAH, S., NAZ, M. Y., BHATTI, H. N., AHMAD, M., AHMED, E., ULLAH, S., & HUS-SIEN, M. (2022). Recent progress in rare earth oxides and carbonaceous materials modified ZnO heterogeneous photocatalysts for environmental and energy applications. *Journal of Environmental Chemical Engineering*, 10(3), 107762.
- AHMAD, M., AHMAD, M., NAFARIZAL, N., SOON, C., SURIANI, A., MOHAMED, A., & MAMAT, M. (2020). Chemisorbed CO₂ molecules on ZnO nanowires (100 nm) surface leading towards enhanced piezoelectric voltage. *Vacuum*, 182, 109565.
- ALHARTHI, F. A., ALI ALGHAMDI, A., ALANAZI, H. S., ALSYAH, A. A., & AHMAD, N. (2020). Photocatalytic degradation of the light-sensitive organic dyes: methylene blue and rose bengal by using urea derived g-C₃N₄/ZnO nanocomposites. *Catalysts*, 10(12), 1457.
- AMBAYE, T. G., VACCARI, M., PRASAD, S., VAN HULLEBUSCH, E. D., & RTIMI, S. (2022). Preparation and applications of chitosan and cellulose composite materials. *Journal of Environmental Management*, 301, 113850.
- AMETA, R., SOLANKI, M. S., BENJAMIN, S., & AMETA, S. C. (2018). Photocatalysis. In *Advanced oxidation processes for wastewater treatment* (pp. 135-175). Elsevier.
- ARASU, M. V., MADANKUMAR, A., THEERTHAGIRI, J., SALLA, S., PRABU, S., KIM, H.-S., AL-DHABI, N. A., AROKIYARAJ, S., & DURAI PANDIYAN, V. (2019). Synthesis and characterization of ZnO nanoflakes anchored carbon nanoplates for antioxidant and anticancer activity in MCF7 cell lines. *Materials Science and Engineering: C*, 102, 536-540.
- ARIF, U., ALI, F., BAHADER, A., ALI, S., ZADA, A., & RAZIQ, F. (2022). Efficient visible light activities of Ag-modified ZnO/g-C₃N₄ composite for CO₂ conversion. *Inorganic Chemistry Communications*, 145, 109944.
- AZIMI, E. B., BADI, A., & GHASEMI, J. B. (2019). Efficient removal of malachite green from wastewater by using boron-doped mesoporous carbon nitride. *Applied Surface Science*, 469, 236-245.
- BADMUS, K. O., TIJANI, J. O., MASSIMA, E., & PETRIK, L. (2018). Treatment of persistent organic pollutants in wastewater using hydrodynamic cavitation in synergy with advanced oxidation process. *Environmental Science and Pollution Research*, 25, 7299-7314.
- BAHIRAEI, H., AZARAKHSH, S., & GHASEMI, S. (2023). Ternary CoFe₂O₄/g-C₃N₄/ZnO heterostructure as an efficient and magnetically separable visible-light photocatalyst: Characterization, dye purification, and mechanism. *Ceramics International*, 49(12), 21050-21059.
- BAI, S., GAO, C., LOW, J., & XIONG, Y. (2019). Crystal phase engineering on photocatalytic materials for energy and environmental applications. *Nano Research*, 12, 2031-2054.
- BARMAN, S., & BASU, S. (2020). Complete removal of endocrine disrupting compound and toxic dye by visible light active porous g-C₃N₄/H-ZSM-5 nanocomposite. *Chemosphere*, 241, 124981.
- BARRIO, J., VOLOKH, M., & SHALOM, M. (2020). Polymeric carbon nitrides and related metal-free materials for energy and environmental applications. *Journal of Materials Chemistry A*, 8(22), 11075-11116.
- BARUAH, S., & DUTTA, J. (2009). Hydrothermal growth of ZnO nanostructures. *Science and technology of advanced materials*.
- BATRA, V., KAUR, I., PATHANIA, D., & CHAUDHARY, V. (2022). Efficient dye degradation strategies using green synthesized ZnO-based nanoplates: A review. *Applied Surface Science Advances*, 11, 100314.
- BELHASSAN, K. (2021). Water scarcity management. In *Water Safety, Security and Sustainability: Threat Detection and Mitigation* (pp. 443-462). Springer.
- BORBÓN, S., LUGO, S., & LÓPEZ, I. (2019). Fast synthesis of ZnO nanoflowers using a conductively heated sealed-vessel reactor without additives. *Materials Science in Semiconductor Processing*, 91, 310-315.
- BORTHAKUR, S., BASYACH, P., KALITA, L., SONOWAL, K., TIWARI, A., CHETIA, P., & SAIKIA, L. (2020). Sunlight-assisted degradation of a pollutant dye in water by a WO₃@ g-C₃N₄ nanocomposite catalyst. *New Journal of Chemistry*, 44(7), 2947-2960.
- BULCHA, B., LETA TESFAYE, J., ANATOL, D., SHANMUGAM, R., DWARAMPUDI, L. P., NAGAPRASAD, N., BHARGAVI, V. N., & KRISHNARAJ, R. (2021). Synthesis of zinc oxide nanoparticles by hydrothermal methods and spectroscopic investigation of ultraviolet radiation protective properties. *Journal of Nanomaterials*, 2021, 1-10.
- CHA, X., YU, F., FAN, Y., CHEN, J., WANG, L., XIANG, Q., DUAN, Z., & XU, J. (2018). Superhydrophilic ZnO nanoneedle array: Controllable in situ

- growth on QCM transducer and enhanced humidity sensing properties and mechanism. *Sensors and Actuators B: Chemical*, 263, 436-444.
- CHAUHAN, A., NEGI, A., KASHYAP, R., SHARMA, B., SHARMA, R. K., & CHAUDHARY, G. R. (2023). Cellulose/chitosan/g-C₃N₄ nano-architected films for visible light induced photocatalytic removal of methylene blue and Cr (VI) from water. *Industrial Crops and Products*, 202, 117113.
- CHAWLA, A., SUDHAIAK, A., RAIZADA, P., AHAMAD, T., VAN LE, Q., NGUYEN, V.-H., THAKUR, S., MISHRA, A. K., SELVASEMBIAN, R., & SINGH, P. (2023). Bi-rich Bi₂O₃/Br₂-based photocatalysts for energy conversion and environmental remediation: A review. *Coordination Chemistry Reviews*, 491, 215246.
- CHEGENI, M., & DEGHAN, N. (2020). Preparation of phosphorus doped graphitic carbon nitride using a simple method and its application for removing methylene blue. *Physical Chemistry Research*, 8(1), 31-44.
- CHI, N., YUAN, X., & SUN, W. (2022). ZnO/g-C₃N₄ Nanostructured Photocatalyst for Enhancement of Photodegradation of Antibiotic Pollutant in Wastewater under Simulated solar Light Illumination. *Int. J. Electrochem. Sci.*, 17(220935), 2.
- CHOI, K.-S., & CHANG, S.-P. (2018). Effect of structure morphologies on hydrogen gas sensing by ZnO nanotubes. *Materials Letters*, 230, 48-52.
- CORONADO, J. M., FRESNO, F., HERNÁNDEZ-ALONSO, M. D., & PORTELA, R. (2013). Design of advanced photocatalytic materials for energy and environmental applications (Vol. 71). Springer.
- CUI, Y., ZHANG, X., ZHANG, H., CHENG, Q., & CHENG, X. (2019). Construction of BiOOH/g-C₃N₄ composite photocatalyst and its enhanced visible light photocatalytic degradation of amido black 10B. *Separation and Purification Technology*, 210, 125-134.
- DEONIKAR, V. G., REDDY, K. K., CHUNG, W.-J., & KIM, H. (2019). Facile synthesis of Ag₃PO₄/g-C₃N₄ composites in various solvent systems with tuned morphologies and their efficient photocatalytic activity for multi-dye degradation. *Journal of Photochemistry and Photobiology A: Chemistry*, 368, 168-181.
- DEVARAYAPALLI, K., VATTIKUTI, S. P., SREEKANTH, T., YOO, K. S., NAGAJYOTHI, P., & SHIM, J. (2020). Hydrogen production and photocatalytic activity of g-C₃N₄/Co-MOF (ZIF-67) nanocomposite under visible light irradiation. *Applied Organometallic Chemistry*, 34(3), e5376.
- DHULL, P., SUDHAIAK, A., SHARMA, V., RAIZADA, P., HASIJA, V., GUPTA, N., AHAMAD, T., NGUYEN, V.-H., KIM, A., & SHOKOUHIMEHR, M. (2023). An overview on InVO₄-based photocatalysts: Electronic properties, synthesis, enhancement strategies, and photocatalytic applications. *Molecular Catalysis*, 539, 113013.
- DUTTA, V., SINGH, P., SHANDILYA, P., SHARMA, S., RAIZADA, P., SAINI, A. K., GUPTA, V. K., HOSSEINI-BANDEGHARAEI, A., AGARWAL, S., & RAHMANI-SANI, A. (2019). Review on advances in photocatalytic water disinfection utilizing graphene and graphene derivatives-based nanocomposites. *Journal of Environmental Chemical Engineering*, 7(3), 103132.
- DUTTA, V., SUDHAIAK, A., KHAN, A. A. P., AHAMAD, T., RAIZADA, P., THAKUR, S., ASIRI, A. M., & SINGH, P. (2023). GCN/CuFe₂O₄/SiO₂ photocatalyst for photo-Fenton assisted degradation of organic dyes. *Materials Research Bulletin*, 164, 112238.
- FAN, Y., YANG, Y.-N., DING, C., & WANG, H.-J. (2022). Degradation of rhodamine B by g-C₃N₄/MoS₂ composite photocatalyst. *Ferroelectrics*, 595(1), 146-155.
- FENG, S., CHEN, T., LIU, Z., SHI, J., YUE, X., & LI, Y. (2020). Z-scheme CdS/CQDs/g-C₃N₄ composites with visible-near-infrared light response for efficient photocatalytic organic pollutant degradation. *Science of the total environment*, 704, 135404.
- FRONCZAK, M. (2020). Adsorption performance of graphitic carbon nitride-based materials: Current state of the art. *Journal of Environmental Chemical Engineering*, 8(5), 104411.
- GARG, T., KAUR, J., KAUR, P., KUMAR, V., TIKOO, K., KAUSHIK, A., & SINGHAL, S. (2022). An innovative Z-scheme g-C₃N₄/ZnO/NiFe₂O₄ heterostructure for the concomitant photocatalytic removal and real-time monitoring of noxious fluoroquinolones. *Chemical Engineering Journal*, 443, 136441.
- GE, W., LIU, K., DENG, S., YANG, P., & SHEN, L. (2023). Z-scheme g-C₃N₄/ZnO heterojunction decorated by Au nanoparticles for enhanced photocatalytic hydrogen production. *Applied Surface Science*, 607, 155036.
- GEORGE, S., POKHREL, S., XIA, T., GILBERT, B., JI, Z., SCHOWALTER, M., ROSENAUER, A., DAMOISEAUX, R., BRADLEY, K. A., & MÄDLER, L. (2010). Use of a rapid cytotoxicity screening approach to engineer a safer zinc oxide nanoparticle through iron doping. *ACS nano*, 4(1), 15-29.

- GUPTA, N. M. (2017). Factors affecting the efficiency of a water splitting photocatalyst: a perspective. *Renewable and Sustainable Energy Reviews*, 71, 585-601.
- HASHEM, E. M., HAMZA, M. A., EL-SHAZLY, A. N., ABD EL-RAHMAN, S. A., EL-TANANY, E. M., MOHAMED, R. T., & ALLAM, N. K. (2021). Novel Z-Scheme/Type-II CdS@ ZnO/g-C₃N₄ ternary nanocomposites for the durable photodegradation of organics: kinetic and mechanistic insights. *Chemosphere*, 277, 128730.
- HAYAT, A., AL-SEHEMI, A. G., EL-NASSER, K. S., TAHA, T., AL-GHAMDI, A. A., SYED, J. A. S., AMIN, M. A., ALI, T., BASHIR, T., & PALAMANIT, A. (2022). Graphitic carbon nitride (g-C₃N₄)-based semiconductor as a beneficial candidate in photocatalysis diversity. *International Journal of Hydrogen Energy*, 47(8), 5142-5191.
- HE, R., ZHOU, J., FU, H., ZHANG, S., & JIANG, C. (2018). Room-temperature in situ fabrication of Bi₂O₃/g-C₃N₄ direct Z-scheme photocatalyst with enhanced photocatalytic activity. *Applied Surface Science*, 430, 273-282.
- HE, Y., WANG, Y., ZHANG, L., TENG, B., & FAN, M. (2015). High-efficiency conversion of CO₂ to fuel over ZnO/g-C₃N₄ photocatalyst. *Applied Catalysis B: Environmental*, 168, 1-8.
- HUANG, L., BAO, D., LI, J., JIANG, X., & SUN, X. (2021). Construction of Au modified direct Z-scheme g-C₃N₄/defective ZnO heterostructure with stable high-performance for tetracycline degradation. *Applied Surface Science*, 555, 149696.
- HUGHES, W. L., & WANG, Z. L. (2004). Formation of piezoelectric single-crystal nanorings and nanobows. *Journal of the American Chemical Society*, 126(21), 6703-6709.
- IMRAN, M., HAIDER, S., AHMAD, K., MAHMOOD, A., & AL-MASRY, W. A. (2017). Fabrication and characterization of zinc oxide nanofibers for renewable energy applications. *Arabian Journal of Chemistry*, 10, S1067-S1072.
- JANG, E., KIM, D. W., HONG, S. H., PARK, Y. M., & PARK, T. J. (2019). Visible light-driven g-C₃N₄@ ZnO heterojunction photocatalyst synthesized via atomic layer deposition with a specially designed rotary reactor. *Applied Surface Science*, 487, 206-210.
- JIA, J., WANG, Y., XU, M., QI, M.-L., WU, Y., & ZHAO, G. (2020). MOF-derived the direct Z-scheme g-C₃N₄/TiO₂ with enhanced visible photocatalytic activity. *Journal of Sol-Gel Science and Technology*, 93, 123-130.
- JIANG, L., YUAN, X., ZENG, G., LIANG, J., CHEN, X., YU, H., WANG, H., WU, Z., ZHANG, J., & XIONG, T. (2018). In-situ synthesis of direct solid-state dual Z-scheme WO₃/g-C₃N₄/Bi₂O₃ photocatalyst for the degradation of refractory pollutant. *Applied Catalysis B: Environmental*, 227, 376-385.
- JIANG, Z., ZHANG, X., CHEN, H. S., HU, X., & YANG, P. (2019). Formation of g-C₃N₄ nanotubes towards superior photocatalysis performance. *ChemCatChem*, 11(18), 4558-4567.
- JOSEPH, S., ABRAHAM, S., PRIYANKA, R. N., ABRAHAM, T., SURESH, A., & MATHEW, B. (2019). In situ S-doped ultrathin g-C₃N₄ nanosheets coupled with mixed-dimensional (3D/1D) nanostructures of silver vanadates for enhanced photocatalytic degradation of organic pollutants. *New Journal of Chemistry*, 43(26), 10618-10630.
- JOURSHABANI, M., SHARIATINIA, Z., & BADI, A. (2017). Facile one-pot synthesis of cerium oxide/sulfur-doped graphitic carbon nitride (g-C₃N₄) as efficient nanophotocatalysts under visible light irradiation. *Journal of colloid and interface science*, 507, 59-73.
- JUNG, H., PHAM, T.-T., & SHIN, E. W. (2019). Effect of g-C₃N₄ precursors on the morphological structures of g-C₃N₄/ZnO composite photocatalysts. *Journal of Alloys and Compounds*, 788, 1084-1092.
- KANAPARTHI, S., & SINGH, S. G. (2020). Highly sensitive and ultra-fast responsive ammonia gas sensor based on 2D ZnO nanoflakes. *Materials Science for Energy Technologies*, 3, 91-96.
- KARRI, R. R., RAVINDRAN, G., & DEGHANI, M. H. (2021). Wastewater—sources, toxicity, and their consequences to human health. In *Soft computing techniques in solid waste and wastewater management* (pp. 3-33). Elsevier.
- KENNEDY, O. W., COKE, M. L., WHITE, E. R., SHAFER, M. S., & WARBURTON, P. A. (2018). MBE growth and morphology control of ZnO nanobelts with polar axis perpendicular to growth direction. *Materials Letters*, 212, 51-53.
- KHERA, S., & CHAND, P. (2019). Influence of different solvents on the structural, optical, impedance and dielectric properties of ZnO nanoflakes. *Chinese journal of physics*, 57, 28-46.
- KONG, J.-Z., ZHAI, H.-F., ZHANG, W., WANG, S.-S., ZHAO, X.-R., LI, M., LI, H., LI, A.-D., & WU, D. (2017). Visible light-driven photocatalytic performance of N-doped ZnO/g-C₃N₄ nanocomposites. *Nanoscale research letters*, 12(1), 1-10.

- KONG, X., WEI, C., ZHU, Y., COHEN, P., & DONG, J. (2018). Characterization and modeling of catalyst-free carbon-assisted synthesis of ZnO nanowires. *Journal of Manufacturing Processes*, 32, 438-444.
- KUMAR, B. (2021). Green synthesis of gold, silver, and iron nanoparticles for the degradation of organic pollutants in wastewater. *Journal of Composites Science*, 5(8), 219.
- KUMAR, R., SUDHAIAK, A., SONU, A., RAIZADA, P., NGUYEN, V.-H., VAN LE, Q., AHAMAD, T., THAKUR, S., HUSSAIND, C. M., & SINGH, P. (2023). Integrating K and P co-doped g-C₃N₄ with Zn-Fe₂O₄ and graphene oxide for S-scheme-based enhanced absorption coupled photocatalytic real wastewater treatment. *Chemosphere*, 139267.
- KUMAR, R., TIWARI, S., THAKUR, V., & PRATAP, R. (2020). Growth of ultrafast, super dense ZnO nanorods using microwaves for piezoelectric MEMS applications. *Materials Chemistry and Physics*, 255, 123607.
- KUMARESAN, N., SINTHIYA, M. M. A., KUMAR, M. P., RAVICHANDRAN, S., BABU, R. R., SETHURMAN, K., & RAMAMURTHI, K. (2020). Investigation on the g-C₃N₄ encapsulated ZnO nanorods heterojunction coupled with GO for effective photocatalytic activity under visible light irradiation. *Arabian Journal of Chemistry*, 13(1), 2826-2843.
- LE, S., ZHU, C., CAO, Y., WANG, P., LIU, Q., ZHOU, H., CHEN, C., WANG, S., & DUAN, X. (2022). V₂O₅ nanodot-decorated laminar C₃N₄ for sustainable photodegradation of amoxicillin under solar light. *Applied Catalysis B: Environmental*, 303, 120903.
- LEE, H.-Y., CHENG, C.-Y., & LEE, C.-T. (2020). Bottom gate thin-film transistors using parallelly lateral ZnO nanorods grown by hydrothermal method. *Materials Science in Semiconductor Processing*, 119, 105223.
- LEE, J.-T., LEE, S.-W., & WEY, M.-Y. (2022). S-scheme g-C₃N₄/ZnO heterojunction photocatalyst with enhanced photodegradation of azo dye. *Journal of the Taiwan Institute of Chemical Engineers*, 134, 104357.
- LEELAVATHI, H., MURALIDHARAN, R., ABIRAMI, N., TAMIZHARASAN, S., SANKEETHA, S., KUMARASAMY, A., & ARULMOZHI, R. (2023). Construction of step-scheme g-C₃N₄/Co/ZnO heterojunction photocatalyst for aerobic photocatalytic degradation of synthetic wastewater. *Colloids and Surfaces A: Physicochemical and Engineering Aspects*, 656, 130449.
- LEONARDI, S. G. (2017). Two-dimensional zinc oxide nanostructures for gas sensor applications. *Chemosensors*, 5(2), 17.
- LI, J., WANG, Y., WANG, Y., GUO, Y., ZHANG, S., SONG, H., LI, X., GAO, Q., SHANG, W., & HU, S. (2023). MXene Ti₃C₂ decorated g-C₃N₄/ZnO photocatalysts with improved photocatalytic performance for CO₂ reduction. *Nano Materials Science*.
- LI, L., ZOU, D., XIAO, Z., ZENG, X., ZHANG, L., JIANG, L., WANG, A., GE, D., ZHANG, G., & LIU, F. (2019). Biochar as a sorbent for emerging contaminants enables improvements in waste management and sustainable resource use. *Journal of Cleaner Production*, 210, 1324-1342.
- LI, X., ZHANG, H., HUANG, J., LUO, J., FENG, Z., & WANG, X. (2017). Folded nano-porous graphene-like carbon nitride with significantly improved visible-light photocatalytic activity for dye degradation. *Ceramics International*, 43(17), 15785-15792.
- LIANG, Q., CUI, S., JIN, J., LIU, C., XU, S., YAO, C., & LI, Z. (2018). Fabrication of BiOI@ UIO-66 (NH₂)@ g-C₃N₄ ternary Z-scheme heterojunction with enhanced visible-light photocatalytic activity. *Applied Surface Science*, 456, 899-907.
- LIU, B., BIE, C., ZHANG, Y., WANG, L., LI, Y., & YU, J. (2021). Hierarchically porous ZnO/g-C₃N₄ S-scheme heterojunction photocatalyst for efficient H₂O₂ production. *Langmuir*, 37(48), 14114-14124.
- LIU, C., QIU, Y., ZHANG, J., LIANG, Q., MITSUZAKI, N., & CHEN, Z. (2019). Construction of CdS quantum dots modified g-C₃N₄/ZnO heterostructured photoanode for efficient photoelectrochemical water splitting. *Journal of Photochemistry and Photobiology A: Chemistry*, 371, 109-117.
- LIU, J., LI, Y., HUANG, L., WANG, C., YANG, L., LIU, J., HUANG, C., & SONG, Y. (2021). Fabrication of novel narrow/wide band gap Bi₄O₅I₂/BiOCl heterojunction with high antibacterial and degradation efficiency under LED and sunlight. *Applied Surface Science*, 567, 150713.
- LIU, J., YAN, X.-T., QIN, X.-S., WU, S.-J., ZHAO, H., YU, W.-B., CHEN, L.-H., LI, Y., & SU, B.-L. (2020). Light-assisted preparation of heterostructured g-C₃N₄/ZnO nanorods arrays for enhanced photocatalytic hydrogen performance. *Catalysis Today*, 355, 932-936.
- LIU, L., CHEN, Z., ZHANG, J., SHAN, D., WU, Y., BAI, L., & WANG, B. (2021). Treatment of industrial dye wastewater and pharmaceutical residue

- wastewater by advanced oxidation processes and its combination with nanocatalysts: A review. *Journal of Water Process Engineering*, 42, 102122.
- LIU, L., LUO, X., LI, Y., XU, F., GAO, Z., ZHANG, X., SONG, Y., XU, H., & LI, H. (2018). Facile synthesis of few-layer g-C₃N₄/ZnO composite photocatalyst for enhancing visible light photocatalytic performance of pollutants removal. *Colloids and Surfaces A: Physicochemical and Engineering Aspects*, 537, 516-523.
- LIU, N., LI, T., ZHAO, Z., LIU, J., LUO, X., YUAN, X., LUO, K., HE, J., YU, D., & ZHAO, Y. (2020). From triazine to heptazine: origin of graphitic carbon nitride as a photocatalyst. *ACS Omega*, 5(21), 12557-12567.
- LIU, R., YANG, W., HE, G., ZHENG, W., LI, M., TAO, W., & TIAN, M. (2020). Ag-modified g-C₃N₄ prepared by a one-step calcination method for enhanced catalytic efficiency and stability. *ACS omega*, 5(31), 19615-19624.
- LIU, X., LIU, L., YAO, Z., YANG, Z., & XU, H. (2020). Enhanced visible-light-driven photocatalytic hydrogen evolution and NO photo-oxidation capacity of ZnO/g-C₃N₄ with N dopant. *Colloids and Surfaces A: Physicochemical and Engineering Aspects*, 599, 124869.
- LOW, J., YU, J., JARONIEC, M., WAGEH, S., & ALGHAMDI, A. A. (2017). Heterojunction photocatalysts. *Advanced materials*, 29(20), 1601694.
- LUU THI, L. A., NETO, M. M., VAN, T. P., NGUYEN NGOC, T., NGUYEN THI, T. M., NGUYEN, X. S., & NGUYEN, C. T. (2021). In situ g-C₃N₄@ Zn nanocomposite: one-pot hydrothermal synthesis and photocatalytic performance under visible light irradiation. *Advances in Materials Science and Engineering*, 2021, 1-10.
- MA, S., ZHAN, S., XIA, Y., WANG, P., HOU, Q., & ZHOU, Q. (2019). Enhanced photocatalytic bactericidal performance and mechanism with novel Ag/ZnO/g-C₃N₄ composite under visible light. *Catalysis Today*, 330, 179-188.
- MALIK, R., & TOMER, V. K. (2021). State-of-the-art review of morphological advancements in graphitic carbon nitride (g-CN) for sustainable hydrogen production. *Renewable and Sustainable Energy Reviews*, 135, 110235.
- MANJULA, Y., KUMAR, R. R., RAJU, P. M. S., KUMAR, G. A., RAO, T. V., AKSHAYKRANTH, A., & SUPRAJA, P. (2020). Piezoelectric flexible nanogenerator based on ZnO nanosheet networks for mechanical energy harvesting. *Chemical Physics*, 533, 110699.
- MISHRA, Y. K., & ADELUNG, R. (2018). ZnO tetrapod materials for functional applications. *Materials Today*, 21(6), 631-651.
- MOHANTY, L., PATTANAYAK, D. S., & DASH, S. K. (2021). An efficient ternary photocatalyst Ag/ZnO/g-C₃N₄ for degradation of RhB and MG under solar radiation. *Journal of the Indian Chemical Society*, 98(11), 100180.
- MOORE, D., & WANG, Z. L. (2006). Growth of anisotropic one-dimensional ZnS nanostructures. *Journal of Materials Chemistry*, 16(40), 3898-3905.
- MORKOÇ, H., & ÖZGÜR, Ü. (2008). Zinc oxide: fundamentals, materials and device technology. John Wiley & Sons.
- NEMIWAL, M., ZHANG, T. C., & KUMAR, D. (2021). Recent progress in g-C₃N₄, TiO₂ and ZnO based photocatalysts for dye degradation: Strategies to improve photocatalytic activity. *Science of the total environment*, 767, 144896.
- NIDHEESH, P. V., COURAS, C., KARIM, A. V., & NADAI, H. (2022). A review of integrated advanced oxidation processes and biological processes for organic pollutant removal. *Chemical Engineering Communications*, 209(3), 390-432.
- ÖZGÜR, Ü., AVRUTIN, V., & MORKOÇ, H. (2013). Chapter 16-zinc oxide materials and devices grown by mbe. *Molecular Beam Epitaxy*, 369-416.
- PANDEY, A., KUMAR, R. R., KALIDASAN, B., LAGHARI, I. A., SAMYKANO, M., KOTHARI, R., ABUSORRAH, A. M., SHARMA, K., & TYAGI, V. (2021). Utilization of solar energy for wastewater treatment: Challenges and progressive research trends. *Journal of environmental management*, 297, 113300.
- PANT, B., PARK, M., & PARK, S.-J. (2019). Recent advances in TiO₂ films prepared by sol-gel methods for photocatalytic degradation of organic pollutants and antibacterial activities. *Coatings*, 9(10), 613.
- PATHANIA, D., SHARMA, M., KUMAR, S., THAKUR, P., TORINO, E., JANAS, D., & THAKUR, S. (2021). Essential oil derived biosynthesis of metallic nano-particles: Implementations above essence. *Sustainable Materials and Technologies*, 30, e00352.
- PATTANAYAK, D. S., PAL, D., MISHRA, J., THAKUR, C., & WASEWAR, K. L. (2023). Doped graphitic carbon nitride (g-C₃N₄) catalysts for efficient photodegradation of tetracycline antibiotics in aquatic environments. *Environmental Science and Pollution Research*, 30(10), 24919-24926.
- PAUL, D. R., GAUTAM, S., PANCHAL, P., NEHRA, S. P., CHOUDHARY, P., & SHARMA, A. (2020).

- ZnO-modified g-C₃N₄: a potential photocatalyst for environmental application. *ACS omega*, 5(8), 3828-3838.
- PHAM, T. H., TRAN, M. H., CHU, T. T. H., MYUNG, Y., JUNG, S. H., MAPARI, M. G., & TAEYOUNG, K. (2023). Enhanced photodegradation of tetracycline in wastewater and conversion of CO₂ by solar light assisted ZnO/g-C₃N₄. *Environmental Research*, 217, 114825.
- QAMAR, M. A., SHAHID, S., JAVED, M., SHARIQ, M., FADHALI, M. M., MADKHALI, O., ALI, S. K., SYED, I. S., AWAJI, M. Y., & SHAKIR KHAN, M. (2022). Accelerated Decoloration of organic dyes from wastewater using ternary Metal/g-C₃N₄/ZnO nanocomposites: an investigation of impact of g-C₃N₄ concentration and Ni and Mn doping. *Catalysts*, 12(11), 1388.
- QU, Y., HUANG, R., QI, W., SHI, M., SU, R., & HE, Z. (2020). Controllable synthesis of ZnO nanoflowers with structure-dependent photocatalytic activity. *Catalysis Today*, 355, 397-407.
- RAIZADA, P., SUDHAIR, A., SAINI, A.K., SINGH, P., Synthesis Of Magnetically Separable Graphitic Carbon Nitride Based Photocatalyst And Methods Thereof, Application Number: 201811018238, Shoolini University Solan.
- RAIZADA, P., SUDHAIR, A., SAINI, A.K., SINGH, P., Ag3vo4 Modified Phosphorus And Sulphur Co-Doped Graphitic Carbon Nitride As High-Dispersed Photocatalyst For Phenol Mineralization And E. Coli Disinfection, Application Number: 201811033392, Shoolini University Solan.
- RAJESHWARI, M. R., KOKILAVANI, S., & KHAN, S. S. (2022). Recent developments in architecturing the g-C₃N₄ based nanostructured photocatalysts: Synthesis, modifications and applications in water treatment. *Chemosphere*, 291, 132735.
- RAO, K. M., SUNEETHA, M., ZO, S., DUCK, K. H., & HAN, S. S. (2019). One-pot synthesis of ZnO nanobelt-like structures in hyaluronan hydrogels for wound dressing applications. *Carbohydrate polymers*, 223, 115124.
- REN, B., XU, Y., ZHANG, L., & LIU, Z. (2018). Carbon-doped graphitic carbon nitride as environment-benign adsorbent for methylene blue adsorption: Kinetics, isotherm and thermodynamics study. *Journal of the Taiwan Institute of Chemical Engineers*, 88, 114-120.
- SALEH, S. M. (2019). ZnO nanospheres based simple hydrothermal route for photocatalytic degradation of azo dye. *Spectrochimica Acta Part A: Molecular and Biomolecular Spectroscopy*, 211, 141-147.
- SAYED, M., ZHU, B., KUANG, P., LIU, X., CHENG, B., GHAMDI, A. A. A., WAGEH, S., ZHANG, L., & YU, J. (2022). EPR investigation on electron transfer of 2D/3D g-C₃N₄/ZnO S-scheme heterojunction for enhanced CO₂ photoreduction. *Advanced Sustainable Systems*, 6(1), 2100264.
- SHARMA, R., ALMÁŠI, M., NEHRA, S. P., RAO, V. S., PANCHAL, P., PAUL, D. R., JAIN, I. P., & SHARMA, A. (2022). Photocatalytic hydrogen production using graphitic carbon nitride (GCN): A precise review. *Renewable and Sustainable Energy Reviews*, 168, 112776.
- SHEIKH, M., PAZIROFTEH, M., DEGHANI, M., ASGHARI, M., REZAKAZEMI, M., VALDERRAMA, C., & CORTINA, J.-L. (2020). Application of ZnO nanostructures in ceramic and polymeric membranes for water and wastewater technologies: a review. *Chemical Engineering Journal*, 391, 123475.
- SHI, L., HE, Z., & LIU, S. (2018). MoS₂ quantum dots embedded in g-C₃N₄ frameworks: A hybrid 0D-2D heterojunction as an efficient visible-light driven photocatalyst. *Applied Surface Science*, 457, 30-40.
- SHRESTHA, R., BAN, S., DEVKOTA, S., SHARMA, S., JOSHI, R., TIWARI, A. P., KIM, H. Y., & JOSHI, M. K. (2021). Technological trends in heavy metals removal from industrial wastewater: A review. *Journal of Environmental Chemical Engineering*, 9(4), 105688.
- SIVAPRAKASH, K., INDUJA, M., GOMATHIPRIYA, P., KARTHIKEYAN, S., & UMABHARATHI, S. (2021). Single-step synthesis of efficient nanometric boron carbon nitride semiconductor for photocatalysis. *Materials Research Bulletin*, 134, 111106.
- SUDHAIR, A., HASIJA, V., SELVASEMBIAN, R., AHAMAD, T., SINGH, A., KHAN, A. A. P., RAIZADA, P., & SINGH, P. (2023). Applications of graphitic carbon nitride-based S-scheme heterojunctions for environmental remediation and energy conversion. *Nanofabrication*, 8.
- SUN, M., CHEN, Z., JIANG, X., FENG, C., & ZENG, R. (2019). Optimized preparation of Co-Pi decorated g-C₃N₄@ ZnO shell-core nanorod array for its improved photoelectrochemical performance and stability. *Journal of Alloys and Compounds*, 780, 540-551.
- SUN, M., WANG, Y., SHAO, Y., HE, Y., ZENG, Q., LIANG, H., YAN, T., & DU, B. (2017). Fabrication of a novel Z-scheme g-C₃N₄/Bi₄O₇ heterojunction photocatalyst with enhanced visible light-driven activity toward organic pollutants. *Journal of colloid and interface science*, 501, 123-132.

- SUN, Q., SUN, Y., ZHOU, M., CHENG, H., CHEN, H., DORUS, B., LU, M., & LE, T. (2022). A 2D/3D g-C₃N₄/ZnO heterojunction enhanced visible-light driven photocatalytic activity for sulfonamides degradation. *Ceramics International*, 48(5), 7283-7290.
- SUN, Y., YANG, H., ZHAO, Z., SUEMATSU, K., LI, P., YU, Z., ZHANG, W., & HU, J. (2020). Fabrication of ZnO quantum dots@ SnO₂ hollow nanospheres hybrid hierarchical structures for effectively detecting formaldehyde. *Sensors and Actuators B: Chemical*, 318, 128222.
- THAKUR, S., KAUR, M., LIM, W. F., & LAL, M. (2020). Fabrication and characterization of electrospun ZnO nanofibers; antimicrobial assessment. *Materials Letters*, 264, 127279.
- TITCHOU, F. E., ZAZOU, H., AFANGA, H., EL GAAYDA, J., AKBOUR, R. A., NIDHEESH, P. V., & HAMDANI, M. (2021). An overview on the elimination of organic contaminants from aqueous systems using electrochemical advanced oxidation processes. *Journal of Water Process Engineering*, 41, 102040.
- TUDOSE, I. V., VRINCEANU, N., PACHIU, C., BUCUR, S., PASCARIU, P., RUSEN, L., KOUDOUMAS, E., & SUCHEA, M. P. (2019). Nanostructured ZnO-based materials for biomedical and environmental applications. In *Functional Nanostructured Interfaces for Environmental and Biomedical Applications* (pp. 285-305). Elsevier.
- VAN THUAN, D., NGUYEN, T. B., PHAM, T. H., KIM, J., CHU, T. T. H., NGUYEN, M. V., NGUYEN, K. D., AL-ONAZI, W. A., & ELSHIKH, M. S. (2022). Photodegradation of ciprofloxacin antibiotic in water by using ZnO-doped g-C₃N₄ photocatalyst. *Chemosphere*, 308, 136408.
- VINAYAGAM, V., MURUGAN, S., KUMARESAN, R., NARAYANAN, M., SILLANPÄÄ, M., DAI VIET, N. V., KUSHWAHA, O. S., JENIS, P., POTDAR, P., & GADIYA, S. (2022). Sustainable adsorbents for the removal of pharmaceuticals from wastewater: A review. *Chemosphere*, 300, 134597.
- WANG, F., LI, W., GU, S., LI, H., LIU, X., & REN, C. (2017). Visible-light-driven heterojunction photocatalysts based on g-C₃N₄ decorated La₂Ti₂O₇: Effective transportation of photogenerated carriers in this heterostructure. *Catalysis Communications*, 96, 50-53.
- WANG, J. (2023). Construction of ternary heterostructured Ag/Ag₂O@ ZnO@ g-C₃N₄ nanocomposite as an widened visible light photocatalyst for the organic oxidation. *Journal of Physics and Chemistry of Solids*, 180, 111389.
- WANG, J., XIA, Y., ZHAO, H., WANG, G., XIANG, L., XU, J., & KOMARNENI, S. (2017). Oxygen defects-mediated Z-scheme charge separation in g-C₃N₄/ZnO photocatalysts for enhanced visible-light degradation of 4-chlorophenol and hydrogen evolution. *Applied Catalysis B: Environmental*, 206, 406-416.
- WANG, J., YANG, Y., & SUN, X. (2016). ZnO disk-like structures and their application in dye sensitized solar cell. *Solid State Communications*, 240, 46-52.
- WANG, N., CHEN, X., JIN, J., ZHANG, P., QIAO, X., & CUI, L. (2020). Tungsten nitride atomic clusters embedded two-dimensional g-C₃N₄ as efficient electrocatalysts for oxygen reduction reaction. *Carbon*, 169, 82-91.
- WANG, P., YANG, M., TANG, S., LI, Y., LIN, X., ZHANG, H., ZHU, Z., & CHEN, F. (2022). Z-scheme heterojunctions composed of 3D graphene aerogel/g-C₃N₄ nanosheets/porous ZnO nanospheres for the efficient photocatalytic reduction of CO₂ with H₂O under visible light irradiation. *Journal of Alloys and Compounds*, 918, 165607.
- WANG, Y., WANG, X., & ANTONIETTI, M. (2012). Polymeric graphitic carbon nitride as a heterogeneous organocatalyst: from photochemistry to multipurpose catalysis to sustainable chemistry. *Angewandte Chemie International Edition*, 51(1), 68-89.
- WANG, Y., YANG, J., JIA, H., YU, M., & JIN, H. (2016). Self-assembled urchin-like ZnO nanostructures fabricated by electrodeposition-hydrothermal method. *Journal of Alloys and Compounds*, 665, 62-68.
- WEI, R., TANG, N., JIANG, L., YANG, J., GUO, J., YUAN, X., LIANG, J., ZHU, Y., WU, Z., & LI, H. (2022). Bimetallic nanoparticles meet polymeric carbon nitride: Fabrications, catalytic applications and perspectives. *Coordination Chemistry Reviews*, 462, 214500.
- WU, Y., WANG, H., TU, W., LIU, Y., TAN, Y. Z., YUAN, X., & CHEW, J. W. (2018). Quasi-polymeric construction of stable perovskite-type LaFeO₃/g-C₃N₄ heterostructured photocatalyst for improved Z-scheme photocatalytic activity via solid pn heterojunction interfacial effect. *Journal of Hazardous Materials*, 347, 412-422.
- XU, C., ANUSUYADEVI, P. R., AYMONTIER, C., LUQUE, R., & MARRE, S. (2019). Nanostructured materials for photocatalysis. *Chemical Society Reviews*, 48(14), 3868-3902.

- YAN, K., & WU, G. (2015). Titanium dioxide microsphere-derived materials for solar fuel hydrogen generation. *ACS Sustainable Chemistry & Engineering*, 3(5), 779-791.
- YANG, Y., & BIAN, Z. (2021). Oxygen doping through oxidation causes the main active substance in g-C₃N₄ photocatalysis to change from holes to singlet oxygen. *Science of the total environment*, 753, 141908.
- YOUNAS, F., MUSTAFA, A., FAROOQI, Z. U. R., WANG, X., YOUNAS, S., MOHY-UD-DIN, W., ASHIR HAMEED, M., MOHSIN ABRAR, M., MAITLO, A. A., & NOREEN, S. (2021). Current and emerging adsorbent technologies for wastewater treatment: trends, limitations, and environmental implications. *Water*, 13(2), 215.
- YU, B., MIAO, C., WANG, D., LI, H., SUN, D., JIANG, W., LIU, C., & CHE, G. (2022). Preparation of visible light responsive g-C₃N₄/H-TiO₂ Z-scheme heterojunction with enhanced photocatalytic activity for RhB degradation. *Journal of Materials Science: Materials in Electronics*, 33(22), 17587-17598.
- YU, T., LIU, Q., CHEN, G., LIU, L., ZHANG, J., GAO, C., & YANG, T. (2022). Microbial coupled photocatalytic fuel cell with a double Z-scheme g-C₃N₄/ZnO/Bi₄O₅Br₂ cathode for the degradation of different organic pollutants. *International Journal of Hydrogen Energy*, 47(6), 3781-3790.
- YUAN, Y., HUANG, G.-F., HU, W.-Y., XIONG, D.-N., ZHOU, B.-X., CHANG, S., & HUANG, W.-Q. (2017). Construction of g-C₃N₄/CeO₂/ZnO ternary photocatalysts with enhanced photocatalytic performance. *Journal of Physics and Chemistry of Solids*, 106, 1-9.
- ZHANG, C., JIA, M., XU, Z., XIONG, W., YANG, Z., CAO, J., PENG, H., XU, H., XIANG, Y., & JING, Y. (2022). Constructing 2D/2D N-ZnO/g-C₃N₄ S-scheme heterojunction: efficient photocatalytic performance for norfloxacin degradation. *Chemical Engineering Journal*, 430, 132652.
- ZHANG, J.-Y., MEI, J.-Y., YI, S.-S., & GUAN, X.-X. (2019). Constructing of Z-scheme 3D g-C₃N₄-ZnO@graphene aerogel heterojunctions for high-efficient adsorption and photodegradation of organic pollutants. *Applied Surface Science*, 492, 808-817.
- ZHANG, L., ZHANG, J., YU, H., & YU, J. (2022). Emerging S-scheme photocatalyst. *Advanced materials*, 34(11), 2107668.
- ZHANG, S., SU, C., REN, H., LI, M., ZHU, L., GE, S., WANG, M., ZHANG, Z., LI, L., & CAO, X. (2019). In-situ fabrication of g-C₃N₄/ZnO nanocomposites for photocatalytic degradation of methylene blue: synthesis procedure does matter. *Nanomaterials*, 9(2), 215.
- ZHANG, W., ZHOU, L., SHI, J., & DENG, H. (2018). Synthesis of Ag₃PO₄/G-C₃N₄ composite with enhanced photocatalytic performance for the photodegradation of diclofenac under visible light irradiation. *Catalysts*, 8(2), 45.
- ZHENG, A. L. T., SABIDI, S., OHNO, T., MAEDA, T., & ANDOU, Y. (2022). Cu₂O/TiO₂ decorated on cellulose nanofiber/reduced graphene hydrogel for enhanced photocatalytic activity and its antibacterial applications. *Chemosphere*, 286, 131731.
- ZHONG, Q., LAN, H., ZHANG, M., ZHU, H., & BU, M. (2020). Preparation of heterostructure g-C₃N₄/ZnO nanorods for high photocatalytic activity on different pollutants (MB, RhB, Cr (VI) and eosin). *Ceramics International*, 46(8), 12192-12199.
- ZHU, C., XIAN, Q., YAO, H., CHEN, C., ZOU, W., DUAN, X., JIANG, Z., & WONG, P. K. (2022a). All-solid-state Z-scheme heterostructures of 1T/2H-MoS₂ nanosheets coupled V-doped hierarchical TiO₂ spheres for enhanced photocatalytic activity. *Materials Today Energy*, 23, 100901.
- ZHU, C., YAO, H., LE, S., YIN, Y., CHEN, C., XU, H., WANG, S., & DUAN, X. (2022b). S-scheme photocatalysis induced by ultrathin TiO₂ (B) nanosheets-anchored hierarchical In₂S₃ spheres for boosted photocatalytic activity. *Composites Part B: Engineering*, 242, 110082.
- ZHU, L., LI, H., LIU, Z., XIA, P., XIE, Y., & XIONG, D. (2018). Synthesis of the 0D/3D CuO/ZnO heterojunction with enhanced photocatalytic activity. *The Journal of Physical Chemistry C*, 122(17), 9531-9539.
- ZHU, Q., SHEN, X., WANG, L., ZHU, L., WANG, L., & LIAO, G. (2018). Polyvinylpyrrolidone-assisted growth and optical properties of ZnO hexagonal bilayer disk-like microstructures. *Chinese Chemical Letters*, 29(8), 1310-1312.
- ZHU, Y., WANG, L., XU, W., XU, Z., YUAN, J., & ZHANG, G. (2022). ZnO/Cu₂O/g-C₃N₄ heterojunctions with enhanced photocatalytic activity for removal of hazardous antibiotics. *Heliyon*, e12644.





Publisher's note: Eurasia Academic Publishing Group (EAPG) remains neutral with regard to jurisdictional claims in published maps and institutional affiliations.

Open Access. This article is licensed under a Creative Commons Attribution-NoDerivatives 4.0 International (CC BY-ND 4.0) licence, which permits copy and redistribute the material in any medium or format for any purpose, even commercially. The licensor cannot revoke these freedoms as long as you follow the licence terms. Under the following terms you must give appropriate credit, provide a link to the license, and indicate if changes were made. You may do so in any reasonable manner, but not in any way that suggests the licensor endorsed you or your use. If you remix, transform, or build upon the material, you may not distribute the modified material. To view a copy of this license, visit <https://creativecommons.org/licenses/by-nd/4.0/>.